AN ABSTRACT OF THE THESIS OF

John Christian Moser for the degree of Master of Science

in Oceanography presented on May 21, 1979

Title: SEDIMENTATION AND ACCUMULATION RATES OF NAZCA PLATE METALLIFEROUS SEDIMENTS BY HIGH RESOLUTION Ge(Li) GAMMA-RAY SPECTROMETRY OF URANIUM SERIES ISOTOPES

Redacted for privacy

Abstract approved:

Sedimentation and accumulation rates were derived for twelve metalliferous sediment cores from the Nazca Plate in the Southeast Pacific. Within the area studied, the highest sedimentation rates occur on the East Pacific Rise (EPR) at 20° South (0.39 - 1.91 cm/10^3 yrs.). Sedimentation rates decrease both along the Rise to 30° South (0.28 - 0.39 cm/10^3 yrs.) and within the deeper Bauer, Yupanqui, and Roggeveen Basins to the east (0.13 - 0.26 cm/10^3 yrs.). The determination of sedimentation rate was greatly facilitated by a modification of the excess Th-230 sedimentation rate technique involving the gamma-ray spectrometric measurement of Pb-214 using a high-resolution, Ge(Li) gamma-radiation detector. One standard deviation counting statistics for the 352 KeV Pb-214 gamma energy peak were accurate to within plus or minus 3% or better. The Pb-214 activity depth profiles actually define the depth distribution of radium in these metalliferous sediments, and the data support the conclusion that no processes, including Ra-226

migration and diffusion, have significantly altered the secular equilibrium between Th-230, Ra-226, and Pb-214 below the surface 12-15 cms of the sediment column.

Accumulation rate patterns indicate that:

1) Hydrothermal sedimentation concentrates Fe, Mn, Si, Al, Cu, Zn, and to a lesser extent, Ni and Ba at the rise crest;

2) Si, Ba, and perhaps Al are biogenous, and at 30° South calcite accumulation decreases linearly with increasing depth consistent with the lysocline model of calcite dissolution;

3) Detrital sources add Si and Al nearest South America and may influence the distribution of all the elements analyzed, except Ca, in these eastern areas; and

4) Hydrogenous processes may influence the relative amounts of Ba and Si in the Bauer Basin.

The skewness of Fe and Mn accumulation patterns near the rise crest implies that bottom currents are flowing eastward across the EPR at 30° South and westward at 20° South. The interaction of these bottom currents with hydrothermal precipitates may also be responsible for the concentration of Th-230 and U at the rise crest.

Sedimentation and Accumulation Rates of Nazca Plate Metalliferous Sediments by High Resolution Ge(Li) Gamma-Ray Spectrometry of Uranium Series Isotopes

by

John Christian Moser

A THESIS

submitted to

Oregon State University

in partial fulfillment of
the requirements for the
degree of

Master of Science

Completed May 21, 1979

Commencement June 1980

APPROVED:

Redacted for privacy

Professor of Oceanography
in charge of major

Redacted for privacy

Dean of School of Oceanography

Redacted for privacy

Dean of Graduate School

Date thesis is presented May 21, 1979

Typed by Karen Bland for John Christian Moser

ACKNOWLEDGEMENTS

I would like to take this opportunity to acknowledge the patience, encouragement, and advice of both Dr. John B. Corliss, my thesis advisor, and Dr. Jack Dymond during the course of this work. My especial thanks go to these two members of my committee for their understanding and support.

Dr. H Herbert Veeh provided the original impetus for the research and offered timely advice and helpful data. Dr. Thomas Beasley made available the gamma radiation detector as well as serving on my committee. I also gratefully acknowledge my other committee members, Dr. Roger Petersen, Dr. James Ingle, and Dr. James Higgins. Dr. David Bukry kindly furnished the coccolith nannofossil stratigraphy data in this study.

I would also like to thank Christin Chou for performing the atomic absorption analyses and Loren Larsen for his helpful introduction into the mysteries of gamma-spectrometry.

Some of the most helpful discussions and criticisms came from my fellow students, especially Mitch Lyle, Debbie Stakes, Bruce Selk, Will Schweller, and Rich Cobler. I was also helped through those long winters and late nights by the good company and smiles of many others along the way : Lindy, Margaret, Chiye, Marty, Dave, Sally, Lynn, Connie, Adolfo, Greg, Marty, Joan, Linda, Gail, Bob, Frances, Lisa, Kathy, Paul, Gretchen, Marilyn, Carlos, Heidi, Clare, Milo, Roger, Larry, and others.

I would like to thank Lindy Zeeman and Karen Bland for their compassion and typing skills and also thank Peggy Lorence for her artistry and friendship. And a certain A. G. Tanner deserves special mention for his dogged determination in keeping my priorities straight. My thanks to everyone.

Books and Men

Imagine yourself in a situation where you are alone, wholly alone on earth, and you are offered one of the two, books or men. I often hear men prizing their solitude, but that is only because there are still men somewhere on earth, even though in the far distance. I knew nothing of books when I came forth from the womb of my mother, and I shall die without books, with another human hand in my own. I do, indeed, close my door at times and surrender myself to a book, but only because I can open the door again and see a human being looking at me.

Martin Buber

TO MY PARENTS

TABLE OF CONTENTS

LIST OF FIGURES

LIST OF TABLES

Sedimentation and Accumulation Rates of Nazca Plate Metalliferous Sediments by High Resolution Ge(Li) Gamma-Ray Spectrometry of Uranium Series Isotopes

INTRODUCTION

Investigations of the Nazca Plate have focused on the origin and distribution of the metalliferous sediments which are associated with the East Pacific Rise (Bostrom and Peterson, 1969; Bostrom, 1973; Dymond et al., 1973; Dymond and Veeh, 1975; McMurtry and Burnett, 1975; Dymond et al., 1976; Heath and Dymond, 1977). The area superficially resembles a typical pelagic sedimentary environment--the detrital input is very low due to the great distances from any continental sources and the physiographic barriers presented by the Peru-Chile Trench and the fossil Galapagos Rise; biogenic flux to the sediment decreases sharply south and west of the equatorial and eastern boundary current upwelling areas especially as one approaches areas with sediment depths exceeding the calcite compensation depth. These deeper basins commonly lack calcium carbonate and siliceous microfossils; rare microfossils are often highly corroded by diagenetic alteration and are unidentifiable (Molina-Cruz, 1978). The Bauer Basin located 600 to 1,200 kms east of the EPR is such a basin and is strongly influenced by hydrogenous sedimentation processes (Heath and Dymond, 1977).

Perhaps the most important aspect of Nazca Plate sedimentation is this proximity to the fast-spreading East Pacific Rise and its associated hydrothermal processes. Anomalously high accumulations of Fe, Mn, U and other metals have been reported from sediments near the crest of

the EPR and the bordering basins, most notably the Bauer Basin (Bender et al., 1971; Dymond and Veeh, 1975; McMurtry and Burnett, 1975).

Extensive geochemical investigations have documented the elemental composition and spatial distribution of these metalliferous sediments (Bostrom and Peterson, 1969; Bonatti et al., 1972; Dymond et al., 1973; Dymond et al., 1976; Heath and Dymond, 1977), but evidence for the sedimentologic sources or the mechanisms and rates of their deposition is limited (Bender et al., 1971; McMurtry and Burnett, 1975; Dymond and Veeh, 1975) especially for those areas south of the Bauer Basin.

Although previous investigations have indicated that these metalliferous sediments are primarily of hydrothermal origin (Dymond et al., 1973), their composition is also governed by additional sources of detrital, hydrogenous and biogenous material (Heath and Dymond, 1977). Accumulation rates (mass/area/time) represent a quantitative mass flux. The geographic accumulation rate patterns of specific elements with unique chemical affinities and behaviors can help define the relative importance of these four sources to the origin and distribution of metalliferous sediments.

We have based our analysis of accumulation rate patterns on twelve metalliferous sediment cores which were collected from the Nazca Plate and form two latitudinal profiles at approximately 20° and 30° South latitude including an additional core from the Bauer Basin near 13° South (see Figure 1). We have calculated accumulation rates for these sediment cores from direct measurement of wet bulk density, water content, elemental composition, and sedimentation rate. The determination of sedimentation rate was greatly facilitated by a modification

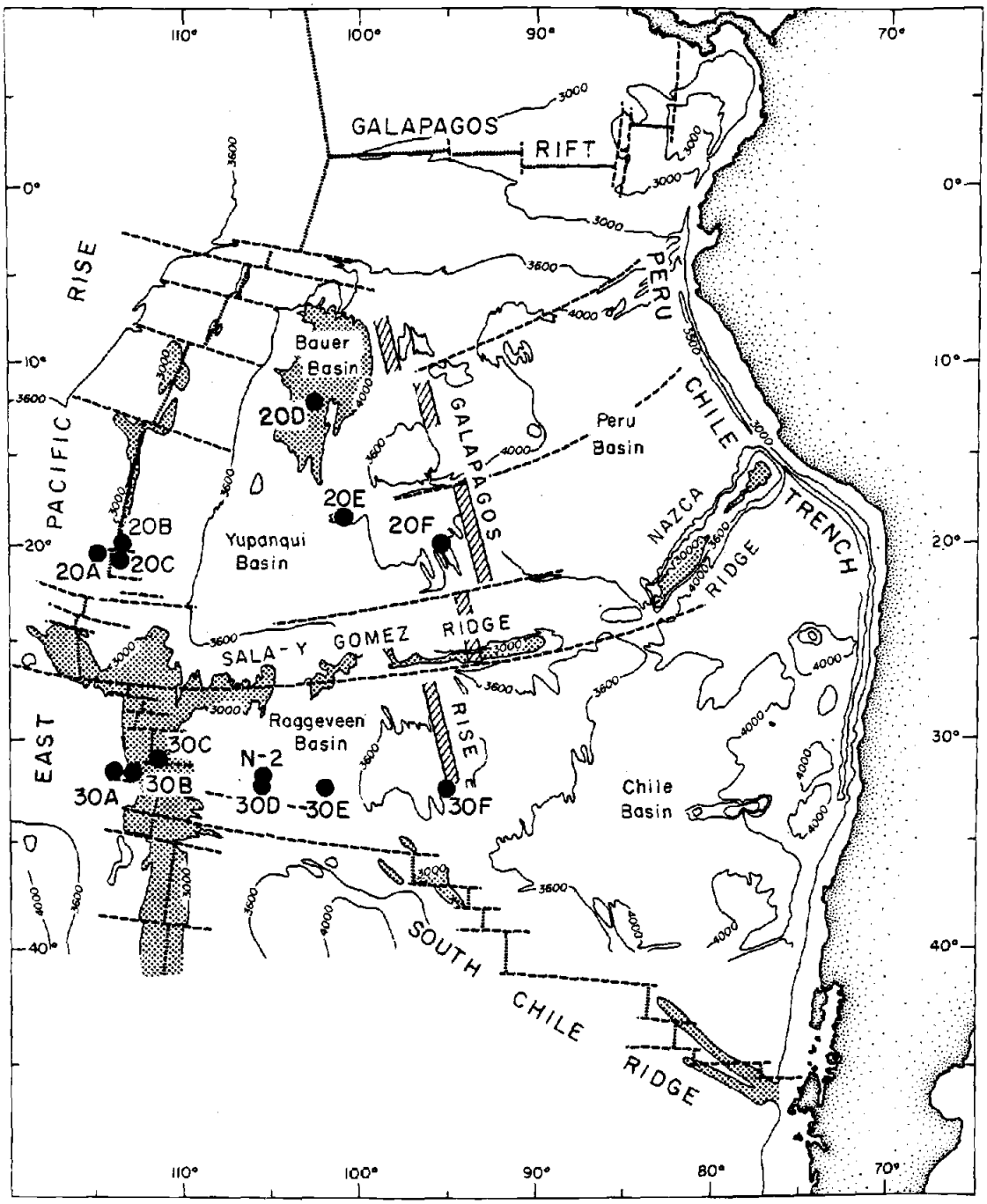

Figure 1. Physiography of the region studied and location of samples used for accumulation rates.

of the excess Th-230 sedimentation rate technique involving the gamma-ray spectrometric measurement of Pb-214 at 352 KeV utilizing a high-resolution, high-efficiency Ge(Li) gamma-ray detector. Further analysis of the Pb-214 activity depth profiles from selected cores also yielded information about the uranium content and the behavior of radium in metalliferous sediments. Using the Pb-214 gamma sedimentation rates for these cores and sediment composition and density data, we have calculated bulk, carbonate, noncarbonate, and elemental Ca, Al, Si, Fe, Mn, Cu, Ni, Zn, and Ba accumulation rates. The geographic accumulation rate patterns of these specific elements and Th-230 can be used to understand the extent and variability of the sedimentologic and geochemical processes affecting metalliferous sediments.

SEDIMENTATION RATE MODEL

Geochemical investigations have indicated that Th-230 enters at a constant rate into ocean waters from the decay of its homogeneously dissolved parent, U-234; Th-230 is then hydrolyzed in seawater, chemically fractionated from the U-234, and precipitated to the sediments at a constant rate (Petterson, 1937; Isaac and Picciotto, 1953; Goldberg and Koide, 1962; Ku et al., 1968; Krishnaswami, 1976; and others). In addition, if the sedimentation rate for the independently accumulating sediment remains constant, then any variation in the concentration (activity) of Th-230 with depth in a core is due solely to its radioactive decay and is simply a function of time.

In the excess Th-230 sedimentation rate method, gamma-ray analysis for this isotope measures the activity of Bi-214 or Pb-214, radioactive daughter products of Th-230. Previous investigations measured the activity of Bi-214 using a NaI(Tl) detector (Osmond and Pollard, 1967; Scott et al., 1972; Cochran, 1973; Cochran and Osmond, 1974; Cochran and Osmond, 1976). In this study, we obtained more accurate counting statistics (±3% or better) by measuring the gamma activity of Pb-214 with a high-resolution Ge(Li) detector. The portion of the U-238 natural radioactive decay series in Figure 2 shows that Pb-214 is removed from Th-230 by four alpha decays. The activity of Pb-214 will equal that of Th-230 only if the isotopes within that decay series are in secular equilibrium.

In a closed system, secular equilibrium between Th-230 and its longest-lived daughter product, Ra-226 (1,622 year half-life), will

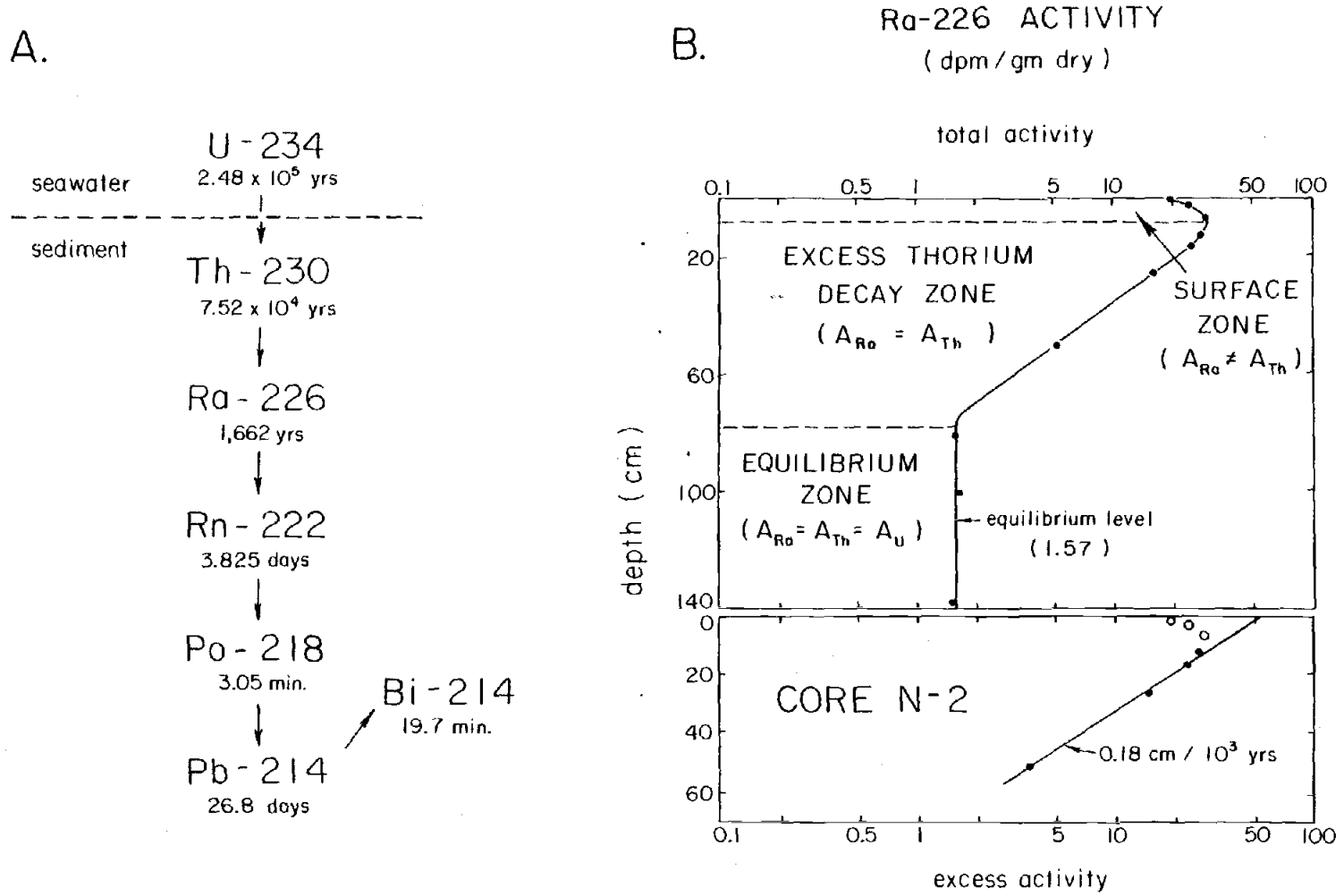

Figure 2. (A) Uranium radioactive decay series isotopes from U-234 to Bi-214 and their half-lives. (Friedlander, Kennedy, and Miller; 1964)

(B) Sedimentation rate model applied to the Pb-214 activity depth profiles using core N-2 as an example. Ra-226 data from Urry,1949. (excess activity = total - equilibrium level activity)

occur in approximately 9,200 years or five to six half-lives of Ra-226. Significant migration of Ra-226 by diffusion out of the sediment during this time could quantitatively affect the equilibrium between Th-230 and Pb-214.

Since the time required for secular equilibrium between Pb-214 and Ra-226 is geologically insignificant, the Pb-214 activity depth profiles measured in this study actually define the depth distribution of Ra-226 within the sedimentary column. The accuracy of the excess Pb-214 sedimentation rate technique is limited by the geochemical behavior of radium within the sediments being dated. For this reason, the sedimentation rate model we chose to best represent the metalliferous cores in this study was derived from the detailed Ra-226 activity profile of core N-2 (Figure 2) a core first described by Urry (1949) and collected from the Nazca Plate very near core 30D (see Figure 1)

The detailed radium activity depth profile of core N-2 reproduced in Figure 2 consists of three zones: a surface radium growth zone, an intermediate excess Th-230 decay zone, and a deeper uranium equilibrium zone. The immediate parent of Ra-226, Th-230, is present in freshly deposited surface sediment greatly in excess of that amount necessary to replenish the radium present in this sediment. Hence, at first, Ra-226 is produced from the Th-230 at a rate in excess of the rate at which radium is decaying. The radium activity increases until secular equilibrium is established between the two elements resulting in a

radium maximum. Theoretically, in a closed system, the time necessary to produce this maximum activity is about 9,200 years. Since the concentration of uranium in deep-sea sediments is normally much less than that necessary to support the Th-230, that "excess" Th-230, and with it the equilibrated Ra-226, decreases in activity until secular equilibrium is established between Th-230 and the uranium in the sample. No further measurable change occurs in this uranium-supported Th-230 activity with time due to the extremely long half-life of U-238. Since the half-life of Th-230 is 75,200 years, equilibrium between Th-230 and uranium is established after five to six half-lives or about 300,000 to 400,000 years.

In actuality, the distribution of radium in surface sediments is highly variable. Biological and physical processes such as bioturbation, current resuspension, and the possible diffusion and migration of radium can all affect this surface sediment and invalidate the closed-system, secular equilibrium between Th-230 and Ra-226 essential to the sedimentation rate method. Beneath an area of high biological productivity in the Panama Basin, recent evidence (Cobler, in prep.) even suggests that there is excess Ra-226 not in equilibrium with Th-230 in surface sediments near the Galapagos Spreading Center. For these reasons, we calculated reliable sedimentation rates using activity data from only the excess Th-230 section beneath the Ra-226 maximum which is essentially a closed system exhibiting secular equilibrium.

The determination of a sedimentation rate from this excess Th-230 interval utilizes the exponential decay of that Th-230 not supported by secular equilibrium with uranium. In alpha spectrometry, the total

Th-230 activity minus the U-234 activity equals the excess Th-230 activity. Although it is sometimes not possible to directly measure the activity of uranium by gamma-ray spectrometry, we calculated equivalent excess activity values by subtracting the uranium-supported, equilibrium-level activity from each sample's total activity. This technique assumes that the uranium concentration is constant throughout the excess activity interval.

As shown in Figure 2, the sedimentation rate (S) is inversely proportional to the slope (B) of the best-fit, linear regression through the excess activity data according to the equation:

$$S = (0.693/T_{230})(-1/B)$$

where T_{230} = the 75,200 year half-life of Th-230.

SAMPLING PROCEDURE

The sampling procedure was determined solely by the need to acquire Pb-214 activity data from both the upper, "excess" interval and the equilibrium level deeper in the core. Piston core and multiple gravity core samples were 10-15 centimeters in length; Kasten box core samples were six centimeters long. After removing a subsample for bulk density determinations, the core sample was carefully collected, homogenized to a 400-500 milliliter volume with double-distilled, de-ionized water and transferred to a plastic Marinelli counting container which was then sealed tightly with vinyl tape. The Marinelli beaker and sediment were left undisturbed for at least two weeks to allow the Ra-226 to re-equilibrate with Pb-214 after the loss of gaseous Rn-222, an intermediate daughter product, during sampling and homogenization. The sample was then placed on the lead-shielded 76 cm^3 Canberra Ge(Li) gamma-radiation detector (15% efficiency - FWHM resolution of 1.97 KeV at 1.33 MeV) and counted for 8×10^4 seconds in the standard Marinelli counting geometry.

The Ge(Li) detector was intercalibrated within one standard deviation counting statistics to a dry powered sample split of Canadian Radioactive Standard Reference Ore BL-2. Preliminary results on a dry sediment standard #4350 supplied by the National Bureau of Standards also gave comparable results. Prior to analyzing samples for this study, experiments were conducted to determine if the calculated activity of any sediment sample was altered by 1) variable water content which could significantly affect the self absorption of the sample; 2) fluctuations in the filling geometry of the Marinelli beakers between 400 and 500 milliliters significantly changing the determined efficiency calibrations;

or 3) the possibility that the plastic used to fabricate the Marinelli counting container was permeable to radon or leaked radon through improperly sealed cracks between top and bottom, thus invalidating the closed system assumption essential for secular equilibrium conditions within the sealed container.

The results of the Canadian Radioactive Reference Ore calibration ruled out the possibility of any significant radon permeability or leakage. Freeze-dried and wet bulk sediment gamma activities at both 400 ml and 500 ml Marinelli geometries were identical within one standard deviation error. Thus, slight variations in water content or counting geometry produced insignificant variability in the counting statistics during the course of the present study.

To determine accumulation rates for each core, the wet bulk density, water content, and elemental concentration data were averaged from the same set of excess Pb-214 sediment samples previously used to delineate the mean sedimentation rate. The wet bulk density and water content were determined for the appropriate sediment samples and averaged. One of the remaining oven-dried, bulk density sediment pellets from each sample was then lightly disaggregated in a mortar and pestle and combined in equal proportion by weight with similar pellets from the same core. This composite "average" sediment sample was then analyzed for Al, Si, Ca, Mn, Fe, Cu, Ni, Zn, and Ba by atomic absorption. Sample and standard preparation and laboratory techniques are described in detail in Fukui (1976).

RESULTS AND DISCUSSION

Sedimentation Rates

Pb-214 Activity Profiles and Behavior of Radium

The total and excess Pb-214 activity depth profiles in Figure 3 were constructed from the data in Table 1.

Except for cores 20D and 30F, the total Pb-214 activity profiles are composite core profiles formed by using both near-surface samples from the multiple gravity core (M) and deeper samples from the companion piston core (P). Cores 20D and 30F are single Kasten box cores. It is apparent from Figure 3 that at core sites 30A through 30E and site 20E the companion multiple gravity core sample has a higher total Pb-214 activity than does the equivalent-depth piston core sample. A simple explanation is that the piston core did not sample the youngest, surface sediment which is present in the multiple gravity core. The data indicate that six of ten piston cores overpenetrated a minimum of 15 cms (30E) to 65 cms (30A) of the surface sediment relative to their companion multiple gravity cores.

At all composite core sites except 20C, only excess Pb-214 activity data from the multiple gravity core was used to determine the sedimentation rate. At 20C, the two, surface multiple gravity samples were dessicated, fractured, and appeared disturbed, therefore only the piston core samples were regressed in this case.

Table 2 compares the excess Pb-214 sedimentation rates to the results of three other sedimentation rate techniques.

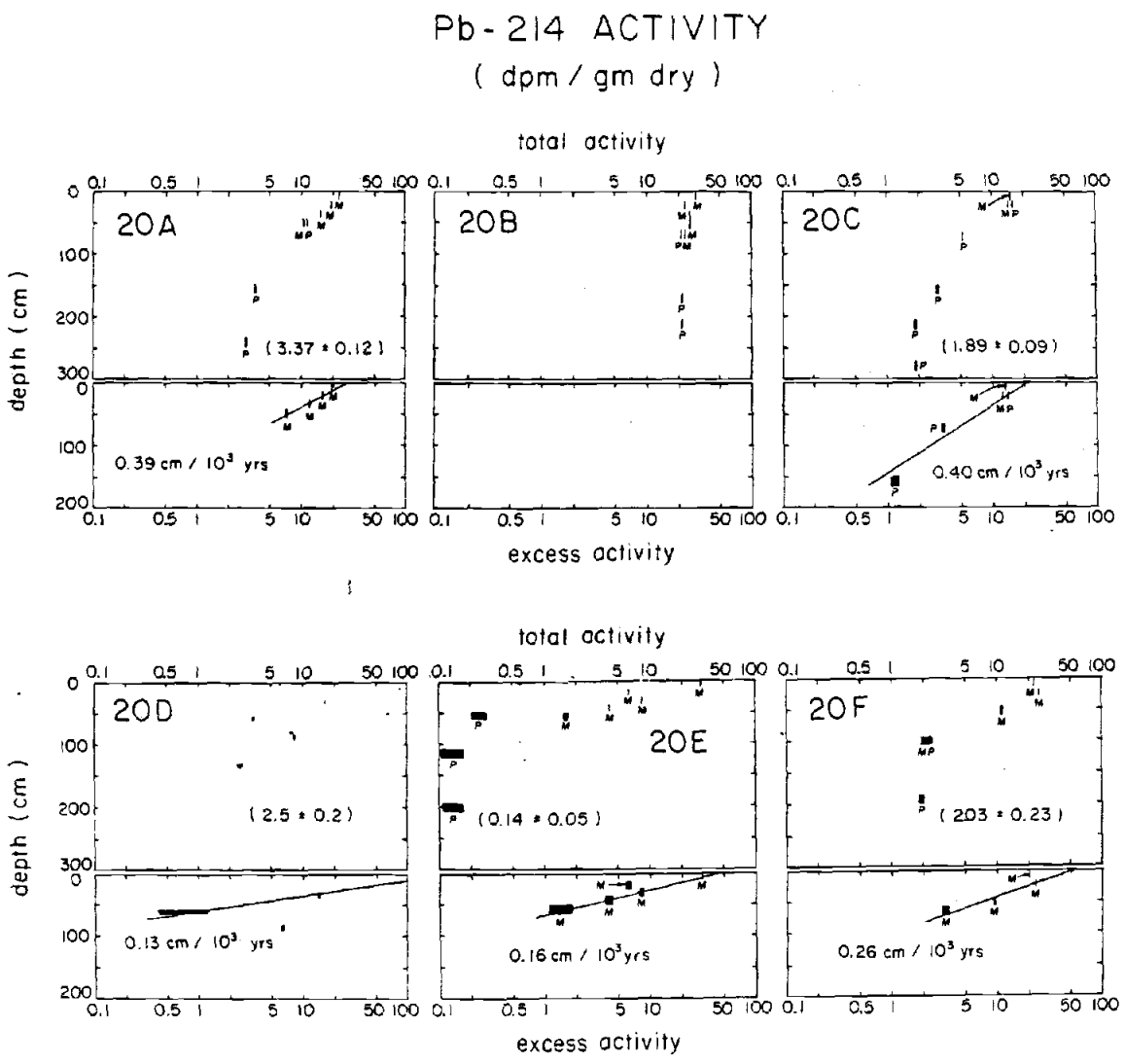

Figure 3. Total and excess Pb-214 activity profiles with Pb-214 gamma sedimentation rates. M = multiple gravity core; P = piston core. (Equilibrium level activity in parentheses.)

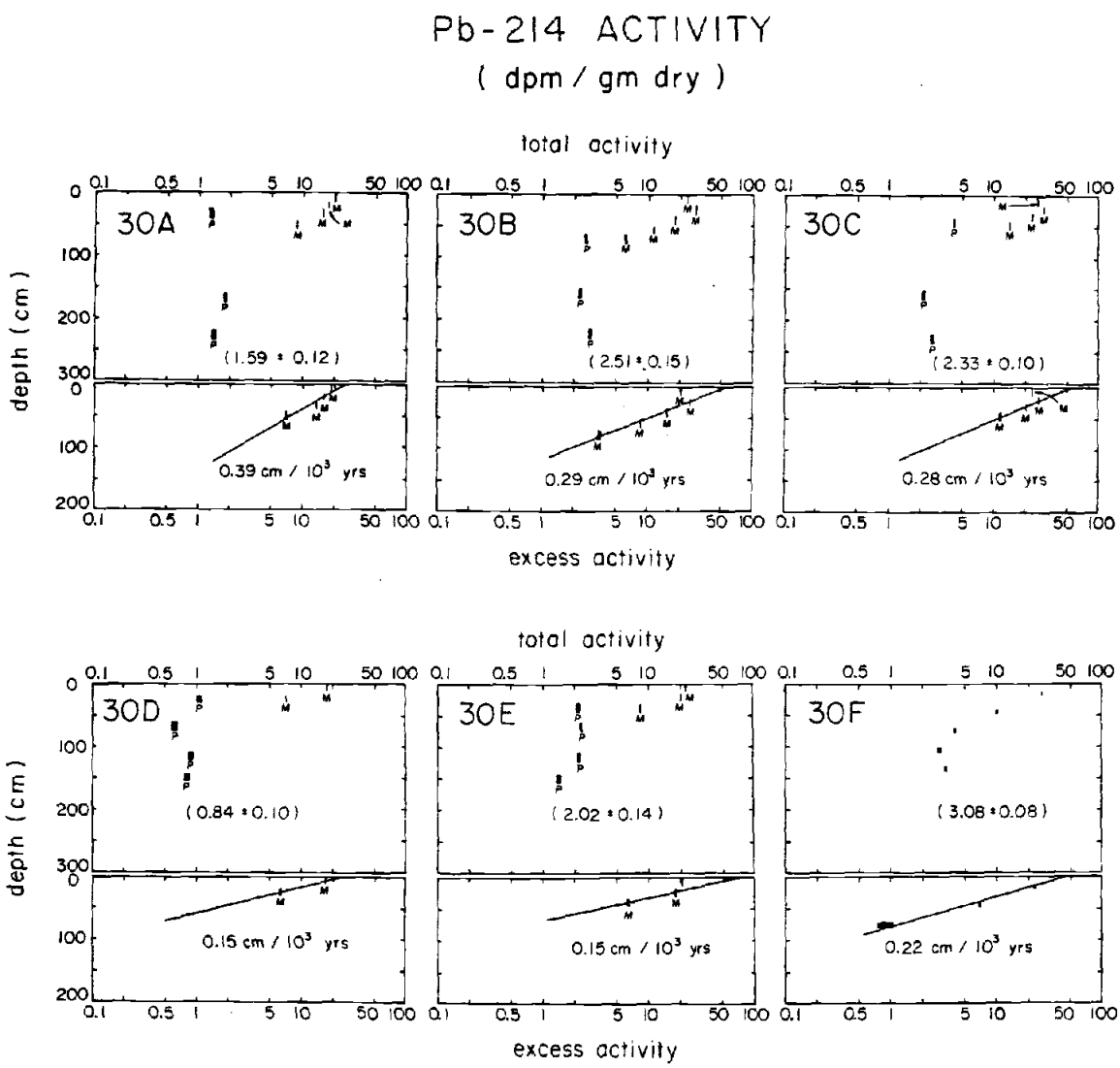

Figure 3. (continued)

Table 1. Total and excess Pb-214 activity data for metalliferous cores in this study .

CORE	DEPTH (cms)	PB-214 GAMMA ACTIVITY (DPM/GM DRY) TOTAL	EXCESS
(20A) OC73-3-25			
MG	(0-15)	22.94 ± 0.22	19.57 ± 0.22
MG	(15-29)	19.31 ± 0.16	15.94 ± 0.20
MG	(29-44)	15.39 ± 0.14	12.02 ± 0.18
MG	(44-59)	10.64 ± 0.13	7.27 ± 0.18
P	(44-59)	11.42 ± 0.12	——
P	(149-164)	3.69 ± 0.09	——
P	(235-250)	3.05 ± 0.08	——
(20B) OC73-3-20			
MG	(0-15)	19.47 ± 0.21	——
MG	(15-30)	14.74 ± 0.23	——
MG	(30-45)	16.32 ± 0.20	——
MG	(45-60)	16.74 ± 0.18	——
MG	(60-75)	14.82 ± 0.19	——
P	(60-75)	13.05 ± 0.19	——
P	(160-175)	13.82 ± 0.19	——
P	(200-215)	13.63 ± 0.21	——
(20C) OC73-3-16			
MG	(0-15)	15.42 ± 0.16	13.53 ± 0.18
MG	(15-27)	14.62 ± 0.15	12.73 ± 0.18
P	(15-27)	16.10 ± 0.15	14.21 ± 0.18
P	(65-80)	5.31 ± 0.07	3.42 ± 0.12
P	(150-165)	3.06 ± 0.06	1.17 ± 0.11
P	(205-220)	1.88 ± 0.06	——
P	(270-285)	1.89 ± 0.06	——

Table 1. (continued)

CORE	DEPTH (cms)	PB-214 GAMMA ACTIVITY (DPM/GM DRY) TOTAL	EXCESS
(20D) Y73-3-21K			
	(8-14)	87.02 ± 0.55	84.5 ± 0.6
	(32-38)	16.57 ± 0.24	14.1 ± 0.3
	(58-64)	3.32 ± 0.16	0.8 ± 0.3
	(88-94)	8.52 ± 0.20	6.0 ± 0.4
	(132-138)	2.53 ± 0.17	——
(20E) OC73-3-8			
	MG (0-12)	31.31 ± 0.28	31.17 ± 0.28
	MG (12-24)	6.53 ± 0.10	6.39 ± 0.11
	MG (24-37)	8.66 ± 0.11	8.52 ± 0.12
	MG (37-50)	4.29 ± 0.08	4.15 ± 0.09
	MG (50-62)	1.62 ± 0.06	1.48 ± 0.08
	P (50-62)	0.25 ± 0.04	——
	P (108-123)	0.14 ± 0.04	——
	P (196-208)	0.14 ± 0.03	——
(20F) OC73-3-6			
	MG (0-15)	22.27 ± 0.23	20.24 ± 0.32
	MG (17-29)	25.26 ± 0.25	23.23 ± 0.34
	MG (45-57)	11.37 ± 0.19	9.34 ± 0.30
	MG (59-71)	5.23 ± 0.14	3.20 ± 0.27
	MG (94-106)	1.99 ± 0.12	——
	P (94-106)	2.18 ± 0.15	——
	P (186-198)	1.93 ± 0.12	——

Table 1. (continued)

CORE	DEPTH (cms)	PB-214 GAMMA ACTIVITY (DPM/GM DRY) TOTAL	EXCESS
(30A) Y73-4-34			
MG	(0-15)	20.09 ± 0.18	18.50 ± 0.22
MG	(15-25)	17.46 ± 0.15	15.87 ± 0.19
MG	(25-40)	15.27 ± 0.13	13.68 ± 0.18
MG	(43-58)	8.65 ± 0.11	7.06 ± 0.16
P	(25-40)	1.31 ± 0.05	———
P	(160-175)	1.80 ± 0.07	———
P	(220-235)	1.39 ± 0.06	———
(30B) Y73-4-40			
MG	(0-15)	23.44 ± 0.22	20.93 ± 0.27
MG	(17-32)	28.10 ± 0.18	25.59 ± 0.24
MG	(34-49)	17.83 ± 0.13	15.32 ± 0.20
MG	(51-66)	11.07 ± 0.11	8.56 ± 0.19
MG	(69-84)	5.99 ± 0.11	3.48 ± 0.19
P	(69-84)	2.52 ± 0.08	———
P	(150-165)	2.23 ± 0.08	———
P	(215-230)	2.79 ± 0.10	———
(30C) OC73-3-30			
MG	(0-15)	25.75 ± 0.20	23.42 ± 0.22
MG	(15-27)	29.45 ± 0.22	27.12 ± 0.24
MG	(27-39)	22.92 ± 0.17	20.59 ± 0.20
MG	(39-54)	14.00 ± 0.16	11.67 ± 0.19
P	(35-50)	4.10 ± 0.08	———
P	(150-165)	2.10 ± 0.07	———
P	(220-235)	2.57 ± 0.07	———

Table 1. (continued)

CORE	DEPTH (cms)	PB-214 GAMMA ACTIVITY (DPM/GM DRY) TOTAL	EXCESS
(30D) Y73-4-55			
MG	(0-12)	17.79 ± 0.18	16.95 ± 0.21
MG	(18-30)	7.22 ± 0.12	6.38 ± 0.16
P	(18-30)	1.06 ± 0.06	——
P	(60-75)	0.62 ± 0.04	——
P	(110-122)	0.88 ± 0.05	——
P	(144-156)	0.81 ± 0.05	——
(30E) Y73-4-56			
MG	(0-12)	22.75 ± 0.20	20.73 ± 0.24
MG	(15-27)	20.15 ± 0.19	18.13 ± 0.24
MG	(31-43)	8.46 ± 0.15	6.44 ± 0.21
P	(31-43)	2.14 ± 0.08	——
P	(60-75)	2.32 ± 0.06	——
P	(110-122)	2.21 ± 0.08	——
P	(144-156)	1.42 ± 0.06	——
(30F) Y73-4-64K			
	(12-18)	26.46 ± 0.24	23.38 ± 0.25
	(42-48)	10.05 ± 0.17	6.97 ± 0.16
	(72-78)	3.99 ± 0.12	0.91 ± 0.14
	(102-108)	2.87 ± 0.13	——
	(132-138)	3.29 ± 0.12	——

Table 2. Comparison of Pb-214 gamma, Th-230 alpha, coccolith, and thickness-age sedimentation rates .

ID	CORE	DEPTH (M)	SEDIMENTATION RATES (CM/10^3 YRS) PB-214 GAMMA	TH-230 ALPHA	COCCOLITH	THICKNESS/AGE
20A	OC73-3-16	3,247	0.39±0.01		0.17 - 0.79	
20B	OC73-3-20	3,081	---------	1.91	0.26 - 1.15	3.35
20C	OC73-3-16	3,150	0.40±0.01		0.13 - 0.79	0.44
20D	Y73-3-21K	4,410	0.13±0.01	0.19(0.12*)		
20E	OC73-3-8	4,090	0.16±0.01			
20F	OC73-3-6	4,309	0.26±0.01		0.04 - 0.05	
30A	Y73-4-34	3,292	0.39±0.01			
30B	Y73-4-40	2,793	0.29±0.01		0.08 - 0.38	
30C	OC73-3-30	3,003	0.28±0.01		0.04 - 0.18	0.35
30D	Y73-4-55	3,790	0.15±0.01			
---	N - 2	-----	0.18			
30E	Y73-4-56	3,717	0.15±0.01			
30F	Y73-4-64K	4,128	0.22±0.01	0.43		

*recalculated for 0 - 60 cms depth interval comparable to Pb-214 Gamma sedimentation rate

Excess Pb-214 sedimentation rates were calculated by fitting a weighted linear regression equation of the form: $\ln Y = A + B(X)$, to the data. The independent variable, X, is the logarithmic mean of the sampling interval. In cases where a surface sample was regressed, since the natural logarithm of zero is undefined, the arithmetic mean was calculated instead. The standard error determined for each sedimentation rate (Table 2) was propagated from the dependent variable, $\ln Y \pm (1/Y)\Delta Y$, which is the natural logarithm of the excess Pb-214 activity weighted proportional to its standard error, ΔY.

The tentative rate of 0.15 cm/10^3 years based upon only two data points from core 30D (Figure 3) is substantiated by a 0.18 cm/10^3 years sedimentation rate for neighboring core N-2.

The nine sedimentation rates derived from the linear, exponential decay of excess Pb-214 activity in cores 30A-F, 20A, C, and F (Figure 3) are consistent with our sedimentation rate model and substantiate the following conclusions:

1. There was a constant bulk sedimentation rate and rate of Th-230 deposition to these cores from at least 10,000 years B.P. until approximately 300,000 years B.P.; and

2. For that portion of the metalliferous sediment column below a depth of 12 to 15 centimeters, these results and the more detailed radium activity profile of core N-2 show no evidence of Ra-226 migration. The obvious linearity of the excess Pb-214 activity with increasing depth substantiates the theoretical, exponential decay of excess Th-230 activity and argues that no processes, including Ra-226 migration and diffusion, have significantly altered the secular equilibrium between

Th-230, Ra-226, and Pb-214. The data support the assumption that Th-230, Ra-226, and Pb-214 are in secular equilibrium below the surface 12-15 centimeters of the sediment column and form a closed system essential to the excess Pb-214 sedimentation rate technique.

Three cores, 20B, 20D, and 20E, had irregular Pb-214 activity profiles and will be discussed in the following sections. 20D and 20E each contain one anomalous excess Pb-214 sample which was not included in that core's linear regression, and an excess Pb-214 sedimentation rate was not calculated for core 20B from the crest of the EPR since the data showed no discernible excess and equilibrium Pb-214 activity sections (see Figure 3).

Comparison of Pb-214 Gamma Data and Th-230 Alpha Data

The excess Th-230 sedimentation rates in Table 2 were determined by Veeh (pers. comm.) using conventional alpha spectrometry techniques. Figure 4 shows comparable plots of the excess Th-230 data and the excess Pb-214 data from cores 20D and 30F. These two cores offer the most direct verification of the excess Pb-214 gamma sedimentation rate technique.

The excess Th-230 and Pb-214 activity data for 20D (Figure 4) agree quite well considering the different size of sample intervals (6 cm wide Pb-214 samples compared to 2 cm wide Th-230 samples). Both the alpha and gamma activity profiles for 20D show a constant, exponential decay of excess activity through the first three data points and yield essentially identical 0.12 and 0.13 cm/10^3 sedimentation rates, respectively. In sediments below this interval, the sedimentation rate

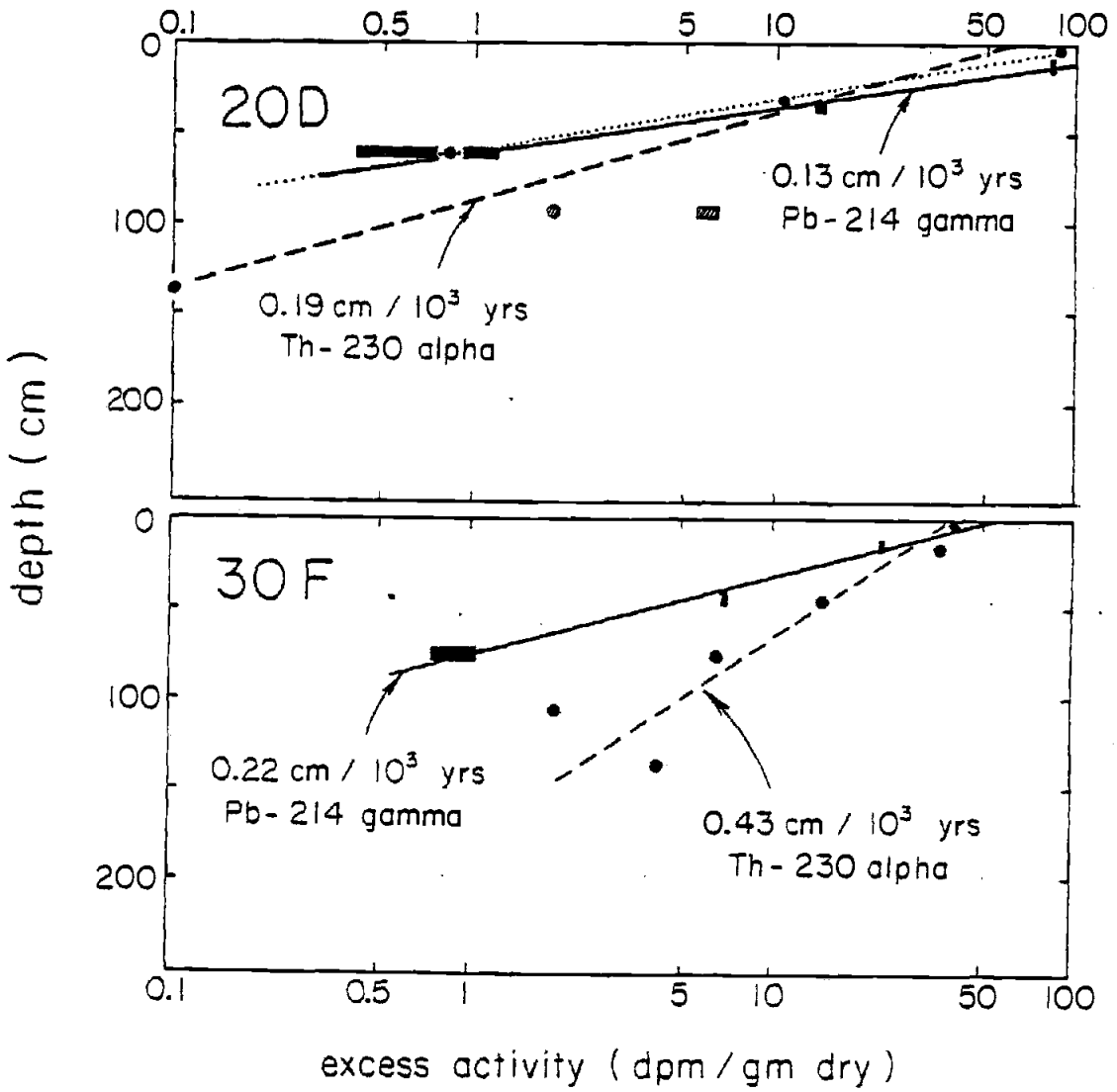

Figure 4. Comparison of Th-230 alpha and Pb-214 gamma data for cores 20D and 30F . (In core 20D, the recalculated 0.12 cm/10^3yrs Th-230 alpha sedimentation rate is shown by a dotted line.)

conditions were significantly different near 90 cms depth and produced an enhanced, excess activity sample in both data sets. We have reported the constant 0.13 cm/10^3 years sedimentation rate for the interval above 60 cms depth; Veeh averaged older sedimentation rate fluctuations below 60 cms into the 0.19 cm/10^3 years Th-230 alpha rate.

The respective excess gamma and alpha data for core 30F in Figure 4 yield sedimentation rates which agree within 50% (Th-230 alpha: 0.43 cm/10^3 years; Pb-214 gamma: 0.22 cm/10^3 years). The Pb-214 gamma technique assumes that the uranium-supported, equilibrium activity below 75 cms depth is constant throughout the entire core; however, Veeh's alpha data show that the uranium concentration steadily decreases from an average of 4.17 ppm U below 75 cms depth to 2.56 ppm U at the core surface. Subtracting the exaggerated Pb-214 equilibrium activity from the upper three samples produced anomalously low excess Pb-214 activities and the lower Pb-214 gamma sedimentation rate. However, the uncertainty in the sedimentation rate for 30F does not affect the conclusions drawn from the accumulation rate patterns discussed later.

Additional Coccolith and Thickness-Age Sedimentation Rates

Coccolith sedimentation rates (Table 2) were determined by Bukry (pers. comm.) who correlated select smear slides of core samples from 20A, B, C, and F and from 30B and C to the coccolith nannofossil stratigraphy determined for DSDP Leg 32 cores (Bukry, 1975). Cores 20A,

20C, and 30B show excellent agreement with the Pb-214 data, and 30C is comparable within 36% of the Pb-214 sedimentation rate. The high 0.26-1.15 cm/10^3 years rate for 20B compares favorably with Veeh's Th-230 alpha rate of 1.91 cm/10^3 years. The disagreement for core 20F is due to the fact that the slower coccolith sedimentation rate was averaged over 635 cms of core, while the more rapid excess Pb-214 rate applies only to the upper 100 cms.

Thickness-age sedimentation rates (Table 2) were computed using the total sediment thickness and the magnetic anomaly age of the underlying oceanic crust (Rea, 1976a, 1976b, 1977, 1978). Only sediment cores that "bottomed out" in basalt as evidenced by a bent piston core barrel, or a mangled or lost core-cutting head, or basalt fragments in the core cutter or core catcher were used. This thickness-age sedimentation rate technique was applied to cores 20B, 20C, and 30C from the present study and to seven additional Nazca Plate cores from near the crest of the East Pacific Rise. Cores 20C and 30C agree within 10% and 20%, respectively, of the Pb-214 sedimentation rates.

Evidence for Slumping at Site 20E

20E was the only core that was physically disturbed. The multiple gravity core had extensively marbled and mottled sediment intervals and gradational intercalation of high and low carbonate layers. Within the red-clay, metalliferous interval from 12-24 cms depth that exhibited anomalously low excess Pb-214 activity (see Figure 3), an intercalated, high-carbonate section was entirely composed of a species of discoaster presumably extinct since the beginning of the Pleistocene.

Core 20E also has an anomalously low total Pb-214 activity profile . The total Pb-214 equilibrium level activity identified in Figure 3 assumedly represents secular equilibrium with an essentially constant uranium concentration. Compared to the 1.3 and 3.1 ppm uranium concentration range for Pacific pelagic clays reported by Krishnaswami (1976), the equivalent uranium level for the metalliferous cores generally agrees well with 20A and 30F showing slight enrichments. Two cores, however, are quite anomalous--20B is apparently enriched in uranium by nearly an order of magnitude, and 20E is depleted by roughly the same factor. Additional evidence for enhanced uranium concentration in core 20B will be discussed in detail later.

One would expect the sediments at site 20E to change from older, carbonate-rich material deeper in the core to younger, increasingly carbonate-poor, metalliferous material as the area moved horizontally away from the fossil Galapagos Rise and the East Pacific Rise into deeper waters below the calcite compensation depth. Thus, the depleted uranium values for 20E would reflect additional dilution by calcium carbonate material deeper in the core, and slumping of this older, carbonate-rich material into the younger, higher Pb-214 activity metalliferous sediments would account for the anomalously low excess Pb-214 activity sample at 12-24 cms depth.

Unusually Rapid Deposition and Uranium Enrichment at Site 20B

Core 20B was recovered from the immediate crest of the East Pacific Rise within a small-scale survey area near 20° South. The coring station description sheet notes that the piston corer bottomed out in

basalt at 267 cms damaging the core cutter, trapping basalt fragments in the core catcher, and bending the core barrel. This core apparently represents very young oceanic sediment.

Veeh's Th-230 alpha sedimentation rate of 1.91 cm/10^3 years for 20B is the most rapid of any core in this study, five times higher than the rates for 20A and 30C flanking it. The 3.35 cm/10^3 years thickness-age rate also implies rapid sedimentation at 20B as does the identification by Bukry of similar coccolith nannofossil zones in smear slides from the surface (1 cm) and near the bottom (230 cm) of the core (Gephyrocapsa oceanica - Quaternary; 0.2 to 0.9 million years age). All three stratigraphies imply a very rapid depositional history for core 20B either by episodic ponding or simply as a result of a continuous flux of sedimentary components to this site.

Both processes are likely. The core's geographic position would facilitate tectonic disturbance and ponding of sediments similar to axial sediments from the Mid-Atlantic Ridge south of the Vema Fracture Zone as described by VanAndel (1969), and the extremely low carbonate content, 39.8% by weight, relative to the other cores from the crestal survey area (20A--69.0% and 20C--81.6% carbonate) strongly implies excessive dilution at site 20B by another sedimentary component.

Evidence from this study shows that core 20B received a higher flux of uranium-enriched, ferromanganese sediments produced by convective, hydrothermal processes on active spreading rises as modeled by Bonatti (1975) and others. The quantitative gamma-spectrometric data reduction for all seven samples from 20B consistently identified the gamma-radiation peaks characteristic of Th-234 (the immediate daughter product of U-238) and U-235. In contrast, these peaks barely registered above

background in samples from all the other sediment cores analysed in this study. The calculated concentrations of U-238 for 20B multiple gravity core samples are approximately 30 ppm U, similar to the values indicative of hydrothermal deposits (Rydell and Bonatti, 1973 and Bonatti, 1975).

The highly anomalous, near-constant total Pb-214 activity profile for 20B also indicates uranium enrichment under the following condition: if the total Pb-214 activity were in equilibrium with an anomalously high background activity of authigenic uranium, then the Pb-214 activity produced by that uranium would actually increase with depth in the core as this U-238 equilibrated through U-234 to Th-230; at the same time, the activity of the excess Pb-214 (unsupported Th-230) derived from the U-234 dissolved in seawater would be decreasing with depth (age) as the excess Th-230 decayed. The unusually high background uranium activity would mask the diminishing decay of excess Th-230 and produce an invariant Pb-214 activity profile. Bonatti et al. (1971) hypothesized an analogous situation for uranium-enriched, reducing sediments high in organic carbon situated in the eastern equatorial Pacific.

Accumulation Rate Patterns

The elemental analyses used to compute the accumulation rates of elements are listed in Table 3. The standard errors of the measurements are: Al, Mn, Fe, Cu, and Zn (approx. 3% error); Si (approx. 4% error); Ca and Ni (approx. 5% error); and Ba (approx. 8% error). Absolute errors cannot be determined for the bulk density and water content determinations, but multiple measurements from the same sample interval

Table 3. Elemental concentrations of bulk sediment for cores in this study.

CORE	SAMPLE I.D.	AL	CA	SI	BA	FE	MN	CU	NI	ZN
(20A) OC73-3-25	MS2586	0.124	27.887	1.081	0.099	8.162	2.840	382	216	163
(20B) OC73-3-20	MS2587	0.350	16.411	3.142	0.071	17.365	5.141	806	270	348
(20C) OC73-3-16	MS2588	0.211	32.808	0.894	0.072	3.804	1.210	203	174	84
(20D) Y73-3-21K	MS2591	2.594	2.996	12.998	1.361	15.210	5.643	1192	1170	431
(20E) OC73-3-8	MS2589	1.299	27.754	4.415	0.426	2.262	0.852	215	276	73
(20F) OC73-3-6	MS2590	6.481	1.888	20.953	1.070	8.505	2.490	687	782	241
(30A) Y73-4-34	MS2580	0.214	34.789	0.617	0.120	1.929	0.518	100	67	43
(30B) Y73-4-40	MS2581	0.258	29.462	1.235	0.206	7.047	2.083	260	186	144
(30C) OC73-3-30	MS2582	0.239	28.389	1.202	0.142	7.746	2.958	317	172	164
(30D) Y73-4-55	MS2583	0.501	29.798	1.546	0.234	6.112	1.981	354	240	120
(30E) Y73-4-56	MS2584	1.436	20.378	3.731	0.383	12.179	3.780	786	655	244
(30F) Y73-4-64K	MS2585	3.715	5.911	9.289	0.682	18.217	5.237	1210	1002	381

Elemental concentrations expressed as percent dry weight except for the trace elements Cu, Ni, and Zn expressed as ppm.

generally agree within 10 percent.

Table 4 summarizes the accumulation rates for the twelve metalliferous sediment cores. To insure that the accumulation and sedimentation rates were internally consistent, the wet bulk density, water content, and elemental concentration data were averaged from the same set of excess Pb-214 sediment samples used to determine the mean sedimentation rate. Therefore, these accumulation rates reflect recent geochemical and sedimentary processes averaged over no more than the last 300,000 to 400,000 years.

Figures 5 through 7 are profiles of the bulk, $CaCO_3$, non-carbonate, and elemental Ca, Si, Al, Ba, Fe, Mn, Cu, Ni, and Zn accumulation rates at core sites 20A through F and 30A through F plotted against their relative distance from the axis of the East Pacific Rise.

To help interpret the accumulation rate patterns, Figure 8 summarizes the sedimentation rates for the Southeast Pacific Ocean compiled from this study and the following sources (Urry, 1949; Goldberg and Koide, 1962; Blackman and Somayajulu, 1966; Glass et al., 1967; Ku et al., 1968; Ericson and Wollin, 1970; Bender et al., 1971; Geitzenauer, 1972; Dymond and Veeh, 1975; McMurtry and Burnett, 1975; Ninkovich and Shackleton, 1975; CLIMAP, 1977; Dymond et al., 1977; and Molina-Cruz, 1978). The Pb-214 sedimentation rates determined in this study are internally consistent and complement the larger-scale trends mapped by the regional data.

Sedimentation rates are highest in proximity to the South American continent where detrital sources and biogenic input from equatorial and

Table 4. Accumulation rates and Th-230 inventory for cores in this study .

CORE SITE AND LOCATION	DEPTH (M)	SED. RATE ($GM/10^3 yrs$) AVG. ρ_T (GM/CM^3)	AVG. H_2O%	AVG. SALT%	AVG. $CaCO_3$%	ACCUMULATION RATES (COMPONENT) $mgms/cm^2/10^3 yrs$ BULK	CARBONATE	NON CARBONATE	(ELEMENTAL) $mgms/cm^2/10^3 yrs$ AL	CA	SI	BA	FE	MN	$\mu gms/cm^2/10^3 yrs$ CU	NI	ZN	(^{230}Th INVENTORY) $dpm/cm^2/10^3 yrs$ $^{230}Th_A$	$^{230}Th_p$	$^{230}Th_A / ^{230}Th_p$
(20A) OC73-3-25 20°00.0'S 114°31.0'W	3247	0.39	1.48	53	4.0	69	271.28	187.29	83.99	0.34	75.65	2.93	0.27	22.14	7.70	104	59	44	6.44	8.31	0.77
(20B) OC73-3-20 19°14.9'S 113°34.5'W	3081	1.91	1.28	68	7.3	40	782.95	311.77	471.18	2.74	120.49	24.60	0.55	135.96	40.25	631	212	273	22.22	7.88	2.82
(20C) OC73-3-16 20°18.8'S 113°14.4'W	3156	0.40	1.56	45	2.9	82	348.04	283.90	64.14	0.74	114.15	3.11	0.25	13.23	4.21	71	61	29	7.48	8.06	0.93
(20D) Y73-3-21K 13°36.8'S 102°31.5'W	4410	0.13	1.19	76	11.2	6	37.00	2.09	34.91	0.96	1.11	4.81	0.50	5.63	2.09	44	43	16	6.84	11.28	0.61
(20E) OC73-3-8 18°08'S 102°01'W	4090	0.16	1.52	49	3.4	69	123.62	84.94	38.68	1.61	34.31	5.46	0.53	2.80	1.05	27	34	9	3.82	10.46	0.37
(20F) OC73-3-6 20°03.3'S 95°17.7'W	4309	0.26	1.28	67	7.0	3	109.85	3.15	102.15	7.12	2.07	23.02	1.18	9.34	2.74	76	86	27	5.96	11.02	0.54

Table 4. (continued)

CORE SITE AND LOCATION	DEPTH (M)	SED. RATE ($CM/10^3$ yrs) AVG. $\frac{C_T}{(GM/CM^3)}$		AVG. H_2O%	AVG. SALT%	AVG. $CaCO_3$%	ACCUMULATION RATES (COMPONENT) $mgms/cm^2/10^3$ yrs BULK	CARBONATE	NON CARBONATE	(ELEMENTAL) AL	CA	SI	BA	FE	MN	$\mu gms/cm^2/10^3$ yrs CU	NI	ZN	(^{230}Th INVENTORY) $dpm/cm^2/10^3$ yrs $^{230}Th_A$	$^{230}Th_P$	$^{230}Th_A/^{230}Th_P$
(30A) Y73-4-34 31°09'S 113°21'W	3292	0.39	1.66	41	2.4	87	302.20	331.06	51.14	0.82	132.96	2.36	0.46	7.37	1.98	38	26	16	9.34	8.42	1.11
(30B) Y73-4-40 31°07.2'S 112°26.3'W	2793	0.29	1.54	48	3.3	73	231.78	169.34	62.44	0.60	68.29	2.86	0.48	16.33	4.83	60	43	33	11.75	7.14	1.65
(30C) 0673-3-30 30°30.1'S 110°28.1'W	3003	0.28	1.46	52	3.8	70	196.36	138.08	58.28	0.47	55.74	2.36	0.28	15.21	5.81	62	34	32	11.63	7.68	1.51
(30D) Y73-4-55 32°38.1'S 105°54.8'W	3524 (37907)	0.15	1.50	51	3.7	74	110.25	81.49	28.76	0.55	32.86	1.71	0.26	6.74	2.18	39	27	13	2.76	9.70	0.29
(30E) Y73-4-56 32°38.8'S 102°16.1'W	3717	0.15	1.40	58	4.9	50	88.20	44.04	44.16	1.27	17.98	3.29	0.34	10.74	3.34	69	58	22	6.93	9.51	0.73
(30F) Y73-4-64K 32°46.4'S 94°42.0'W	3871	0.22	1.31	67	7.0	13	94.82	12.43	82.39	3.52	5.61	8.81	0.65	17.27	4.97	115	95	36	4.70	10.56	0.45

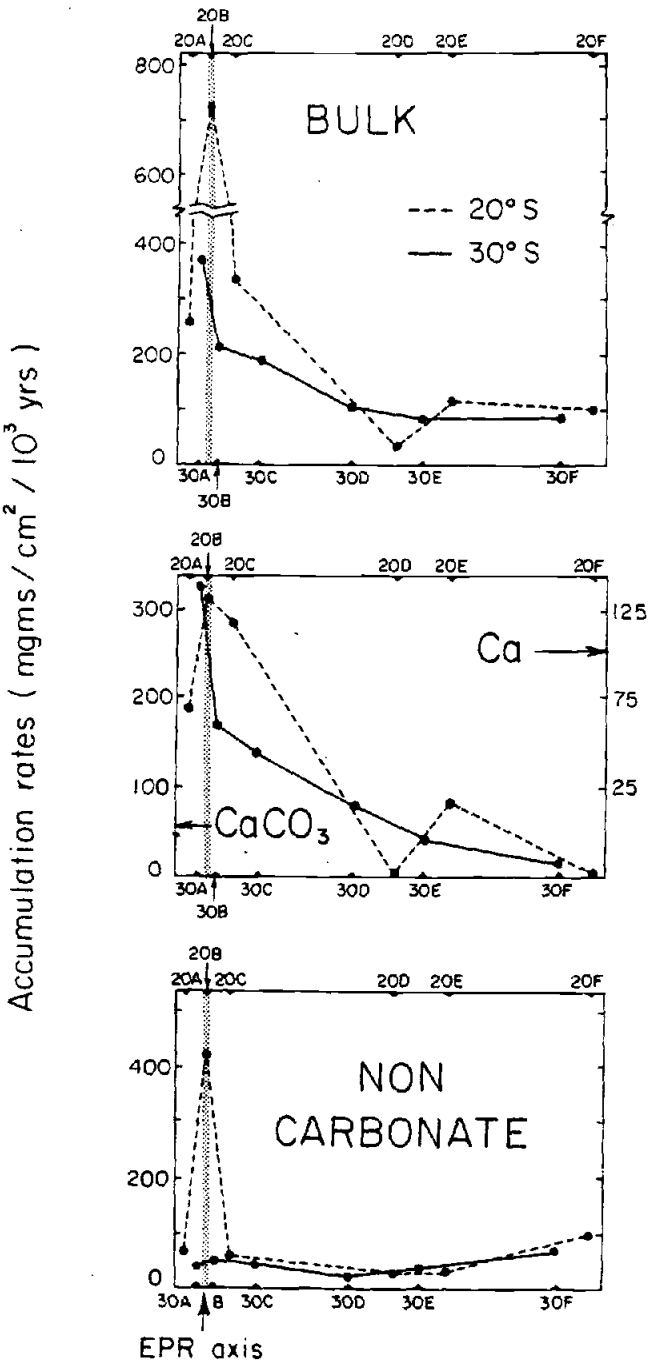

Figure 5. Bulk, carbonate, and non-carbonate accumulation rate profiles for cores 20A - F and 30A - F. ($CaCO_3$ calculated from the Ca content after the procedure in Dymond et al.(1976) .

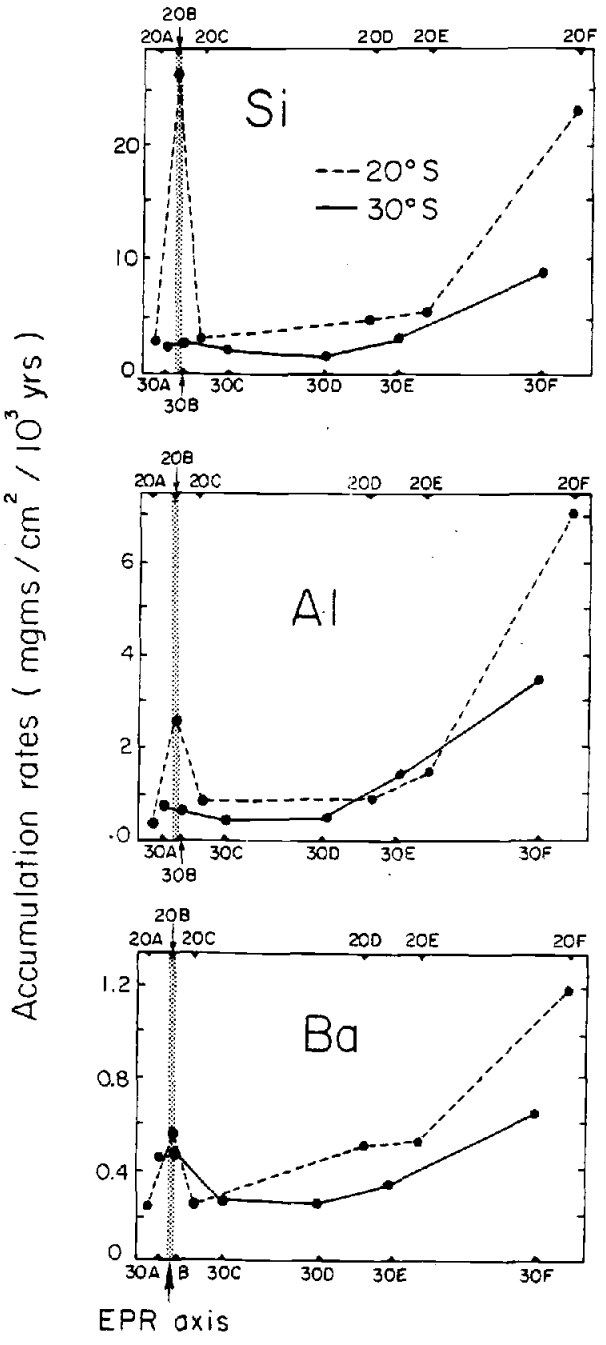

Figure 6. Si, Al, and Ba accumulation rate profiles for cores 20A - F and 30A - F .

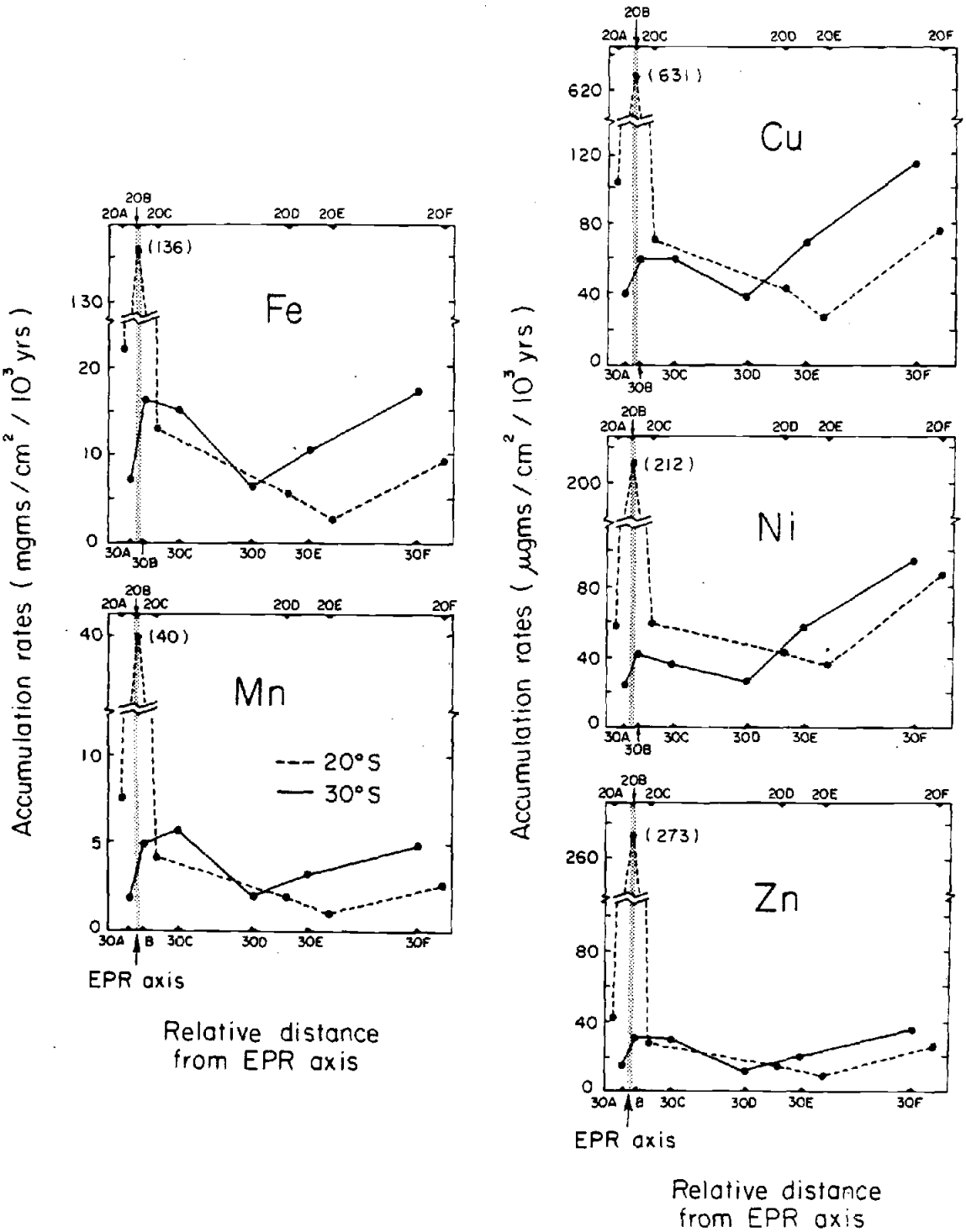

Figure 7. Fe, Mn, Cu, Ni, and Zn accumulation rate profiles for cores 20A - F and 30A - F .

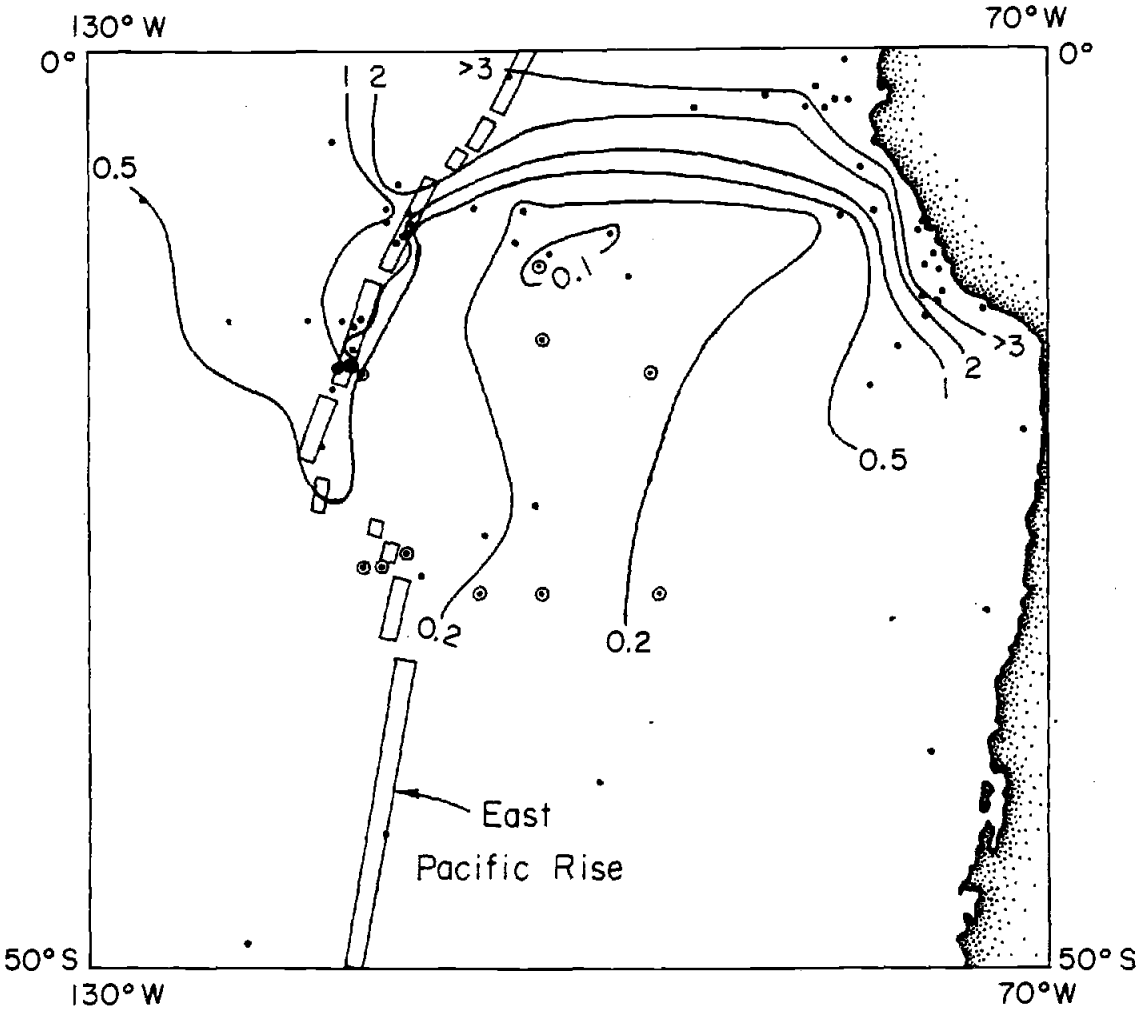

Figure 8. Regional sedimentation rate pattern for the southeast Pacific Ocean . Sedimentation rates are expressed as cm/10^3yrs .(Cores from the present study are circled)

marginal upwelling processes predominate. Sedimentation rates again increase on the East Pacific Rise, especially near the equator, where hydrothermal and biogenous sources become more important. In the relative absence of these three major hydrothermal, biogenous, and detrital sources, authigenic hydrogenous processes can influence the deeper, central basins which exhibit the lowest sedimentation rates, such as the Bauer Basin.

Hydrothermal Sedimentation

Hydrothermal processes should predominate in rise crest cores at active spreading ridges. As discussed previously, 20B is located immediately adjacent to the spreading axis of the East Pacific Rise and has an enhanced uranium concentration indicative of hydrothermal deposits. 20B is accumulating bulk sediment twice as rapidly as any other core in this study (Figure 5), yet has an ambient flux of biogenic carbonate material. This rapid deposition at core 20B is due to its sixfold increase in non-carbonate accumulation (Figure 5) and strongly indicates a dominantly hydrothermal input. The metals Fe, Mn, Cu, Zn, Si, and Al are all enriched six to seven times in 20B relative to adjacent cores, 20A and 20C (Figures 6 and 7), implying some common, hydrothermal process concentrating all six elements near the axis of the EPR. Apparently less influenced by hydrothermal sedimentation, Ni is enriched only by a factor of 3-4, and Ba shows just a twofold increase at 20B.

East of the EPR, Fe, Mn, Cu, Ni, and Zn are all accumulating more rapidly at 30° South than at 20° South (Figure 7). At 30D, E, and F, the accumulation rates of all five elements vary proportionately,

increasing steadily eastward until maximum values at core 30F near the South Chile Ridge. This expansive geographic covariance of Cu, Ni, and Zn with Fe and Mn suggests that these trace metals can be quickly adsorbed onto precipitating, surface-active ferromanganese hydroxyoxides. After the process suggested by Lonsdale (1976) and Heath and Dymond (1977), bottom waters flowing northward through extensive fracture zones associated with the South Chile Ridge could transport hydrothermal ferromanganese hydroxyoxides enriched in Fe, Mn, Cu, Ni, and Zn northward to these three Roggeveen Basin cores. On the rise crest at 30° South, the accumulation patterns of these five elements for cores 30A, B, and C (Figure 7) further suggest that Ni and Zn are preferentially associated with Fe, while Cu covaries more strongly with Mn.

The enhancement of Ba relative to Si at sites 30A and 30B (Figure 6) is similar to the $CaCO_3$ pattern there (Figure 5) and suggests both a hydrothermal and biogenous origin for Ba as described by Bostrom et al. (1973).

Biogenous Sedimentation

With the exception of core 30A, the accumulation of calcium carbonate (calcite) in the 30° South profile decreases linearly with increasing depth (Figure 9). This pattern is consistent with the lysocline model of calcite dissolution under areas of uniform biological productivity and has been reported for equatorial Pacific sediments by Swift and Wenkham (1978) and Heath et al. (1977). The zero intercept at approximately 4,150 meters depth represents the calcite compensation depth for this area (Berger et al., 1976; and Broecker and

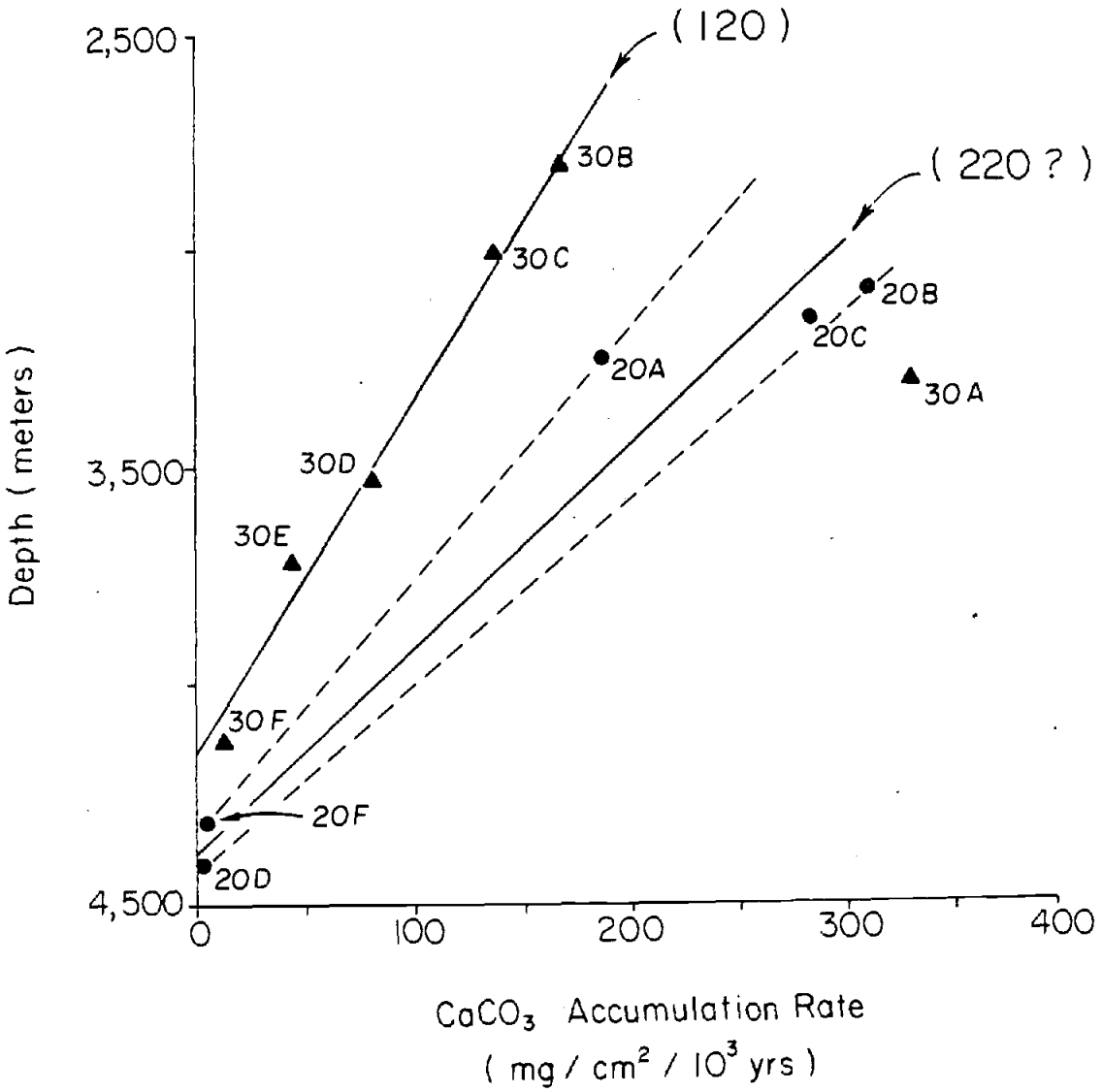

Figure 9. Variation of calcium carbonate (calcite) accumulation rate as a function of water depth for the 20° South and 30° South core profiles . Calcite dissolution gradients (mgms/cm^2/10^3yrs/km water depth) for each profile are in parentheses .

Takahashi, 1978). The calcite dissolution gradient of 120 mg/cm^2/10^3 years/km water depth is much less than those reported for Equatorial Pacific areas and reflects the much less corrosive bottom waters here.

The linear calcite dissolution gradient for the 20° South profile is tentative. Two eastern basin cores, 20D and 20F, lie below the CCD, and core 20E with the unusual occurrences of pre-pleistocene calcareous coccoliths was not plotted.

One interesting speculation, however, is that within both latitudinal profiles the maximum carbonate fluxes at 20B, 20C, and 30A are remarkably similar, perhaps indicating an average, maximum preservation of calcium carbonate of approximately 300 mg/cm^2/10^3 years in this area of the Southeast Pacific central gyre.

In the Southeast Pacific Ocean, the latitudinal deposition pattern of biogenic silica reflects the decreasing productivity north and south of the equator. This gradient is replicated by the accumulation pattern of Si (Figure 6) which shows a higher flux of Si both on and off the rise crest at 20° South than at 30° South. In the eastern basins, Ba, Al, and Si have similar patterns. Their higher values in the 20° South profile (Figure 6) suggest that the distribution of Ba, Si, and to a lesser extent, Al is partially governed by biogenous sources previously indicated by the covariance of Ba and Si in the water column (Chan et al., 1977) and by higher concentrations of Ba and Al beneath areas of enhanced biological productivity (Bostrom et al., 1973; Leinen and Stakes, 1979). However, primarily of biogenous origin, Ba accumulation increases to the east less rapidly than either Si or Al (Figure 6) which suggests

an eastern detrital source for these latter two elements.

Detrital Sedimentation

The significant eastward increase of Si and Al to local maxima in cores 20F and 30F nearest South America (Figure 6) is consistent with a primarily detrital origin for these common terrigenous elements. In the eastern basins, the greater enrichment of Si, Al, and Ba at 20° South than at 30° South could also be due to the presence of a larger detrital source to the north with enhanced aeolian input and surface current circulation contiguous to South America as inferred by Molina-Cruz (1978). It is difficult to differentiate between biogenous and detrital sources in this area. One clue comes from the fact that detrital sources to this area of the ocean have a Si/Al ratio of approximately three (Heath and Dymond, 1977). The Si/Al ratio for cores from this northern profile (computed from Table 3) decreases from maxima at 20° South crestal sites to minimal values near three for the easternmost cores, 20E (3.4) and 20F (3.2) again indicating a detrital contribution in this area.

To a lesser extent, all elements except Ca show increasing accumulation eastward toward South America in both latitudinal profiles (see Figures 5 through 7) and may be influenced to some degree by detrital sources.

Hydrogenous Sedimentation

Hydrogenous processes are governed by low-temperature, authigenic reactions with seawater and should be enhanced in the Bauer Basin, an

area of low bulk accumulation (Figure 5) least affected by hydrothermal, detrital, and biogenous sedimentary material. It is difficult to detect the very slow accumulation of hydrogenous material to these sediments or any diagenetic processes that simply transfer metals from one phase to another. However, if one of two previously related metals is physically or mineralogically fractionated and lost during diagenesis, this change could affect their relative accumulation rates.

Within these limitations, the accumulation of Ba and/or Si may be influenced by hydrogenous processes in the Bauer Basin. Although Ba and Si generally covary east of the rise crest in both latitudinal profiles, Ba is slightly enriched relative to Si in core 20D (Figure 6).

One can speculate that this tentative pattern results from the diagenetic formation of relatively insoluble barite and the dissolution and remobilization of biogenic silica into an Fe-rich smectite phase within the Bauer Basin after the process described by Heath and Dymond (1977).

Geological Evidence for Bottom Current Movement

If one accepts that both Fe and Mn are being injected into the oceanic bottom water from a linear source along the axial crest of the East Pacific Rise in this area, then it follows that as bottom water currents move across the axis, more Fe and Mn should accumulate "downstream" of the axis than "upstream"; i.e., the accumulation of Fe and Mn in sediments near the active spreading axis should be asymetrically skewed in the direction of the average bottom current. In addition, studies by Krauskopf (1957) of the solubilities of Mn and Fe in seawater

showed that Fe should precipitate first followed by Mn. Using a first order scavenging model, Weiss (1977) estimated that the horizontal diffusion for hydrothermal Mn injected at the Galapagos Rift was on the order of 1,000 kms. Following this reasoning, the Mn pattern should have the maximum accumulation skewed even further "downstream" than the more rapidly precipitating Fe hydroxyoxides.

Figure 7 shows that the maximum Mn accumulation pattern is skewed further to the east than that for Fe at cores 30A, B, and C and implies eastward flowing bottom currents on the rise crest at 30° South. Although dominated by core 20B, both Fe and Mn are accumulating more rapidly to the west at site 20A than to the east at 20C, which implies average current movement to the west at 20° South on the EPR.

Concentration of Th-230 at the Rise Crest

By calculating the concentration of excess Th-230 at the sediment surface, one can compute the accumulation rate of Th-230 ($^{230}Th_A$) at each core site. A useful reference index is the expected production rate of Th-230 from uranium dissolved in the seawater column directly above each core site ($^{230}Th_P$) using a uranium concentration of 3.3 ug/l in seawater and a $^{234}U/^{238}U$ ratio of 1.15 (Sackett, 1964).

Previous work (Cochran and Osmond, 1976) had shown that $Th_A < Th_P$ on oceanic highs and $Th_A > Th_P$ in adjacent basins. These authors attributed this pattern to the winnowing of fine-grained material rich in Th from oceanic highs where $Th_A < Th_P$ and deposition of this "surplus" fine fraction (and its adsorbed Th) in adjacent basin sediments where

$Th_A > Th_P$. When Dymond and Veeh (1975) applied this "winnowing" interpretation to their data, the results implied a transport of thorium-rich fines from the Bauer Basin upslope to the crest of the EPR, a pattern contrary to all the other available data! Dymond and Veeh subsequently suggested that the relative enrichment of Th-230 on the EPR was due to surface active ferromanganese hydroxyoxides at the rise crest preferentially scavenging Th-230 supplied from the overlying water column and bottom currents. Dymond and Veeh stated that

> "it seems probable that Sackett's model of Th-230 production and removal in the overlying water column (Sackett, 1964) is too simplistic for this region and that some accounting for bottom-water movement and iron hydroxide scavenging must be made. Even with the slow movement of bottom water, hydrothermal precipitates forming on the rise crest would be effectively bathed by hundreds to thousands of times more water than that in the overlying water column. It is possible that the removal of Th-230 from moving bottom water by Fe and Mn hydroxyoxides formed from hydrothermal solutions is the explanation for the surplus Th-230 deposition observed in the rise crest. Such an explanation necessarily requires that some areas 'downstream' of the bottom flow have $Th_A < Th_P$."

Uranium is also preferentially concentrated at the crest of the East Pacific Rise as shown by Dymond and Veeh (1975) and the results of this study for core 20B. The enrichment of U and Th in hydrothermal deposits is to be expected since, in the laboratory, U and Th are commonly stripped from solution and concentrated by co-precipitation with Fe and Mn hydroxides (Ku, 1966). Several authors (Dymond et al., 1973; Ku, 1969) have suggested that ferromanganese precipitates might be instrumental in concentrating U in hydrothermal deposits.

The Th-230 inventory (Th_A/Th_P) and the accumulation of Th (Th_A) for cores from this study in Table 4 clearly show highest values for those cores nearest the spreading axis of the EPR. The Th-230

inventory and Th accumulation both decrease to the east of the EPR, dropping to minimum values in the deeper eastern basin cores.

It would be interesting to speculate that the concentration of Th and U at the crest of the EPR might deplete bottom waters of these elements and produce the anomalously low Th accumulations at cores 20D, E, and F and 30D, E, and F, especially if bottom waters simply flowed east across the EPR into these deeper eastern basins. However, from an analysis of isotherms at 3,800 meters depth, Lonsdale (1976) inferred that bottom currents move east and south through the EPR and the Bauer Basin to eventually mix near 15° South with bottom waters which have travelled north and west through the South Chile Ridge and the Peru Basin. Also, results of this study infer westward flowing bottom currents at 20° South on the EPR.

Therefore, until more is known about bottom current direction and the accumulation of Th on the South Chile Ridge and to the west of the EPR, there can be only a tentative connection between bottom water movement over active spreading rises in this area and the depleted Th accumulation in these eastern basin cores.

SUMMARY

The Pb-214 activity depth profiles measured in this study actually define the depth distribution of Ra-226 within these metalliferous sediments. For that portion of the metalliferous sediment column below a depth of 12-15 cms, the results of this study argue strongly that no processes, including possible Ra-226 migration and diffusion, have significantly altered the secular equilibrium between Th-230, Ra-226, and Pb-214 essential to the Pb-214 sedimentation rate technique. The data also support a relatively constant bulk sedimentation rate and rate of Th-230 deposition to these metalliferous sediments from at least 300,000 years B.P. until approximately 10,000 years B.P.

For these cores, the Pb-214 gamma sedimentation rate technique is a reliable alternative to the Th-230 alpha method in most cases. Although discrepancies occur in sediments with an unusually high or variable uranium content and in samples where Th-230 and Pb-214 are not in radioactive equilibrium, additional independent sedimentation rate determinations substantiated the Pb-214 rates in six of eight comparisons.

Analysis of accumulation rate patterns shows that uranium-enriched, hydrothermal sediments concentrate Fe, Mn, Si, Al, Cu, Zn, and to a lesser extent, Ni and Ba at the rise crest. The trace metals Cu, Ni, and Zn are adsorbed onto Fe-Mn hydroxyoxides, and bottom water circulation can affect the distribution of these hydrothermal precipitates near the East Pacific Rise and the South Chile Ridge.

The accumulation patterns of Si, Ba, and perhaps Al are partially influenced by biogenous sedimentary material, and at 30° South, calcium

carbonate accumulation decreases linearly with increasing depth, a pattern consistent with the lysocline model of calcite dissolution.

Detrital input enhances Si and Al accumulation nearest South America. To a lesser extent, all elements analysed, except Ca, show a similar eastward increase implying some detrital influence.

The slight enrichment of Ba relative to Si in the Bauer Basin may be due to more pervasive hydrogenous processes there, but the accumulation rate data are highly tentative.

And lastly, the skewness of Fe and Mn accumulation patterns near the rise crest implies that bottom currents are flowing eastward across the EPR at 30° South and westward at 20° South. Interaction of these bottom currents with hydrothermal precipitates may also be responsible for the concentration of Th-230 and U at the rise crest.

BIBLIOGRAPHY

Bender, M., W. Broecker, V. Gornitz, U. Middel, R. Kay, S. S. Sun, and P. Biscaye. 1971. Geochemistry of three cores from the East Pacific Rise. Earth and Planetary Science Letters 12:425-433.

Berger, W. H., C. G. Adelseck, Jr., and L. A. Mayer. 1976. Distribution of carbonate in surface sediments of the Pacific Ocean. Journal of Geophysical Research 81:2617-2627.

Blackman, A. and B.L.K. Somayajulu. 1966. Pacific Pleistocene cores: faunal analyses and geochronology. Science 154:886-889.

Bonatti, E. 1975. Metallogenesis at oceanic spreading centers. Annual Review of Earth and Planetary Sciences 3:401-431.

Bonatti, E., D. E. Fisher, O. Joensuu, and H. S. Rydell. 1971. Post-depositional mobility of some transition elements, phosphorus, uranium, and thorium in deep sea sediments. Geochimica et Cosmochimica Acta 35:189-201.

Bonatti, E., T. Kraemer and H. Rydell. 1972. Classification and genesis of submarine iron-manganese deposits. In: Ferromanganese Deposits on the Ocean Floor, ed. David R. Horn. Lamont-Doherty Geological Observatory, Columbia University, Palisades, New York.

Bostrom, K. and M. N. A. Peterson. 1969. The origin of aluminum-poor ferromanganoan sediments in areas of high heat flow on the East Pacific Rise. Marine Geology 7:427-447.

Bostrom, K. 1973. The origin and fate of ferromanganoan active ridge sediments. Stockholm Contr. Geology 27:149-243.

Bostrom, K. O. Joensuu, C. Moore, B. Bostrom, M. Dalziel and A. Horowitz. 1973. Geochemistry of barium in pelagic sediments. Lithos 6:159-174.

Broecker, W. S. and T. Takahashi. 1978. The relationship between lysocline depth and in situ carbonate ion concentration. Deep Sea Research 25: 65-95.

Bukry, D. 1975. Coccolith and silicoflagellate stratigraphy, northwestern Pacific Ocean, Deep Sea Drilling Project Leg 32. In: Larson, R. L., R. Moberly, et al. 1975. Initial Reports of the Deep Sea Drilling Project, Volume 32, Washington (U.S. Government Printing Office) pp. 677-701.

Chan, L. H., D. Drummond, J. M. Edmond and B. Grant. 1977. On the barium data from the Atlantic GEOSECS expedition. Deep Sea Research 24:613-649.

CLIMAP. 1977. Climap Data Base archived at NGSDC, Boulder, Colorado.

Cochran, J. K. 1973. Sedimentation rate patterns and radium-226 geochemistry of pelagic sediments from the Tasman Basin. Thesis, Florida State University, Tallahassee, Florida. 181 p.

Cochran, J. K. and J. K. Osmond. 1974. Gamma spectrometry of deep-sea cores and sediment accumulation rates. Deep-Sea Research 21:721-737.

Cochran, J. K. and J. K. Osmond. 1976. Sedimentation patterns and accumulation rates in the Tasman Basin. Deep-Sea Research 23:193-210.

Dymond, J. J. B. Corliss, G. R. Heath, C. W. Field, E. J. Dasch and H. H. Veeh. 1973. Origin of metalliferous sediments from the Pacific Ocean. Geological Society of America Bulletin 84:3355-3372.

Dymond, J. and H. H. Veeh. 1975. Metal accumulation rates in the Southeast Pacific and the origin of metalliferous sediments. Earth and Planetary Science Letters 28:13-22.

Dymond J., J. B. Corliss and R. Stillinger. 1976. Chemical composition and metal accumulation rates of metalliferous sediments from Sites 319, 320B, and 321. In: Initial Reports of the Deep Sea Drilling Project, Vol. 34, eds. R. S. Yeats and S. R. Hart et al., U.S. Government Printing Office.

Dymond, J., J. B. Corliss and G. R. Heath. 1977. History of metalliferous sedimentation at Deep Sea Drilling Site 319, in the southeastern Pacific. Geochemica et Cosmochimica Acta 41:741-753.

Ericson, D. B. and G. Wollin. 1970. Pleistocene climates in the Atlantic and Pacific Oceans: a comparison based on deep-sea sediments. Science 167:1483-1485.

Friedlander, G., J. W. Kennedy, and J. M. Miller. 1964. Nuclear and Radiochemistry, Second edition. John Wiley and Sons. 585 p.

Fukui, S. 1976. Laboratory techniques used for atomic absorption spectrophotometric analysis of geologic samples, Reference 76-10, August, 1976. School of Oceanography, Oregon State University, Corvallis, Oregon 97331. 126 p.

Geitzenhauer, K. R. 1972. The Pleistocene calcareous nannoplankton of the Subantarctic Pacific Ocean. Deep-Sea Research 19:45-60.

Glass, B., D. B. Ericson, B. C. Heezen, N. D. Opdyke and J. A. Glass. 1975. Geomagnetic reversals and Pleistocene chronology. Nature 216:437-442.

Goldberg, E. D. and M. Koide. 1962. Geochronological studies of deep-sea sediments by the ionium/thorium method. Geochimica et Cosmochimica Acta 26:417-450.

Heath, G. R. and J. Dymond. 1977. Genesis and transformation of metalliferous sediments from the East Pacific Rise, Bauer Deep, and Central Basin, Northwest Nazca Plate. Geologic Society of America Bulletin 88:723-733.

Heath, G. R., T. C. Moore, Jr., and T. H. VanAndel. 1977. Carbonate accumulation and dissolution in the Equatorial Pacific during the past 45 million years. In: The Fate of Fossil Fuel CO_2 in the Oceans, ed. N. R. Anderson and A. Malahoff. Plenum Publishing Corp., pp. 627-639.

Isaac, N. and E. Picciotto. 1953. Ionium determinations in deep-sea sediments. Nature 171:742-743.

Krauskopv, K. B. 1957. Separation of iron from manganese in sedimentary processes. Geochimica et Cosmochimica Acta 12:61-82.

Krishnaswami, S. 1976. Authigenic transition elements in Pacific pelagic clays. Geochimica et Cosmochimica Acta 40:425-434.

Ku, T. 1966. Uranium series disequilibrium in deep-sea sediments. Unpublished Ph.D. Thesis, Columbia University, New York. 157 p.

Ku, T. 1969. Uranium series isotopes in sediments from the Red Sea hot brine area. In: Hot Brines and Recent Heavy Metal Deposits in the Red Sea, ed. E. T. Degens and D. A. Ross, Springer-Verlag, New York, 512-524.

Ku, T., W. S. Broecker and N. Opdyke. 1968. Comparison of sedimentation rates measured by paleomagnetic and the ionium methods of age determination. Earth and Planetary Science Letters 4:1-16.

Leinen, M. and D. Stakes. 1979. Metal accumulation rates in the central equatorial Pacific during the Cenozoic. Geological Society of America Bulletin 90:357-375.

Lonsdale, P. 1976. Abyssal circulation of the southeastern Pacific and some geological implications. Journal of Geophysical Research 81: 1163-1176.

McMurtry, G. M and W. R. Burnett. 1975. Hydrothermal metallogenesis in the Bauer Deep of the southeastern Pacific. Nature 254:42-44.

Molina-Cruz, A. 1978. Late quarternary oceanic circulation along the Pacific coast of South America. Ph.D. thesis, Oregon State University, Corvallis, Oregon.

Ninkovich, D. and N. J. Shackleton. 1975. Distribution, stratigraphic position and age of ash layer "L", in the Panama Basin region. Earth and Planetary Science Letters 27:20-34.

Osmond, J. K. and Lin D. Pollard. 1967. Sedimentation rate determination in deep sea cores by Gamma-ray spectrometry. Earth and Planetary Science Letters 3:476-480.

Petterson, H. 1937. Das uerhältniss thorium zu uran in den gesteinen und im meer. [The proportion of thorium to uranium in rocks and in the sea.] Anz Akad. Wiss. Wien. Math.-Naturw. Kl., p. 127-128.

Rea, D. K. 1976a. Changes in the axial configuration of the East Pacific Rise near 6°S during the past 2 m.y.. Journal of Geophysical Research 81:1495-1504.

Rea, D. K. 1976b. Analysis of a fast-spreading rise crest: The East Pacific Rise, 9° to 12° South. Marine Geophysical Researches 2:291-313.

Rea, D. K. 1977. Local axial migration and spreading rate variations, East Pacific Rise, 31°S. Earth and Planetary Science Letters 34: 78-84.

Rea, D. K. 1978. Asymetric sea-floor spreading and a nontransform axis offset: The East Pacific Rise 20°S survey area. Geological Society of America Bulletin 89:836-844.

Rydell, H. S. and E. Bonatti. 1973. Uranium in submarine metalliferous deposits. Geochimica et Cosmochimica Acta 37:2557-2565.

Sackett, W. M. 1964. Measured deposition rates of marine sediments and implications for accumulation rates of extraterrestrial dust. Annals of the New York Academy of Sciences 119:239-346.

Scott, M. R., J. K. Osmond, and J. K. Cochran. 1972. Sedimentation rates and sediment chemistry in the South Indian Basin. In: Antarctic Oceanology II - The Australian - New Zealand Sector, Antarctic Research Series, 19, D. E. Hayes, ed., American Geophysical Union, p. 317-334.

Swift. S. A. and C. Wenkham. 1978. Holocene accumulation rates of calcite in the Panama Basin: Lateral and vertical variations in calcite dissolution. Marine Geology 27:67-77.

Urry, W. D. 1949. Radioactivity of ocean sediments. VI. Concentrations of the radioelements in marine sediments of the Southern Hemisphere. American Journal of Science 247:257-275.

Van Andel, T. H. 1969. Recent uplift of the Mid-Atlantic Ridge south of the Vema Fracture Zone. Earth and Planetary Science Letters 7:228-230.

Weiss, R. F. 1977. Hydrothermal manganese in the deep sea: Scavenging residence time and $Mn/^{3}He$ relationships. Earth and Planetary Science Letters 37:257-262.

APPENDICES

APPENDIX A

GENERAL CORE DESCRIPTIONS

In general, the six cores from the two East Pacific Rise crestal survey areas - OC73-3-16, OC73-3-20, and OC73-3-25 from the 20D South area; and Y73-4-34, Y73-4-40, and OC73-3-30 from the 30D South area - were surprisingly comparable in regard to the uniformity of their lithology, color, and texture with depth in each core. All the cores are very uniform to lightly mottled dark yellowish brown silty clay to clayey silt; smear slides are very calcareous with abundant foraminifera, nannofossils, clay particles, and glass fragments and show lesser amounts of calcareous matter and micronodules. Again, these rise crest cores show only slight gradations in these descriptive characteristics with increasing depth in the core. (OC73-3-20 was unique in that it was the only core that contained numerous basalt fragments throughout its length.)

Y73-4-55, Y73-4-56, and Y73-4-64K traverse shallower to deeper depths in the Roggeveen Basin and show a gradation from west to east of decreasing foraminifera content, rare to absent siliceous microfossils such as radiolaria, diatoms, and silicoflagellates, and an increasing red-brown aggregate and zeolite content.

The two easternmost cores from the Yupanqui Basin, OC73-3-8 and OC73-3-6 plus Y73-3-21K from the Bauer Basin are not so easily related and seem to represent individual areas.

OC73-3-8 has the most variable lithology of any of the twelve cores exhibiting moderately to heavily mottled dusky yellowish brown silty clay with occasional foraminifera interlaminated with lighter colored, highly calcareous foram bearing intervals mottled with darker

yellowish brown calcareous silty clay.

OC73-3-6, the easternmost core of the 20D South traverse, is extremely homogeneous throughout 250 centimeters showing dusky yellowish brown clay with occasional yellowish brown mottling. Small flakes tentatively identified as illite and small "peppery" grains (glass?) are present throughout the core. Some sand sized material was noted at approximately 500 centimeters depth and a Mn nodule was also noted in the core.

Y73-3-21K from the Bauer Basin is again extremely homogeneous throughout its 148 centimeter length and is a very dusky red clay with few minor grayish orange mottles. Smear slide showed abundant red brown aggregates, common zeolites, few ash particles, and the absence of forams, coccos, discos, rads, diatoms, and silicoflagellates.

APPENDIX B

CALCULATION OF SEDIMENTATION RATE AND ACCUMULATION RATE

Sedimentation Rate

The decay of excess Th-230 activity below the radium maximum is governed by the simple equation for the decay of a single radioactive element within a closed system:

$$A_{(2)} = A_{(1)} \exp(-\lambda_{230}(t_2 - t_1)) \quad (1)$$

Rewriting equation (1) in terms of the sedimentation rate, S, gives

$$S = \frac{(0.693)(x_2 - x_1)}{(T_{230})(\ln (A_1/A_2))} \quad (2)$$

where

λ_{230} = decay constant of Th-230

T_{230} = half-life of Th-230 (75,200 years)

x_1 = depth in the core equivalent to time, t_1

x_2 = depth in the core equivalent to time, t_2

S = the sedimentation rate over the interval x_2 to x_1

The equation for S can also be written as

$$\ln A_{(2)} = -(0.693/T_{230}*S)(x_2 - x_1) + \ln A_{(1)}$$

which is the equation for a linear function, $y = ax + b$, showing excess activity versus depth with an intercept of $\ln A_{(1)}$ and a slope of $0.693/T_{230}*S$. Since T_{230} is constant, the slope of the line is negative and inversely proportional to the sedimentation rate, S.

Accumulation Rate

If wet bulk density, water content, and sedimentation rate of a core are known, the accumulation rate of any component of the dry bulk sediment is given by:

$$A_C = C_C S \rho_T (1 - X_W)$$

where

A_C = the accumulation of a given component, C (expressed as grams dry sediment/$cm^2/10^3$ years)

C_C = the concentration (weight fraction) of that component in the dry bulk sediment (a unitless ratio)

S = the sedimentation rate over the sampling interval (expressed as $cm/10^3$ years).

ρ_T = the wet bulk density (expressed as grams wet bulk sediment/cm^3)

X_W = the weight fraction of water in the wet bulk sediment (a unitless ratio)

The term $\rho_T(1 - X_W)$ is equivalent to the dry uncompressed bulk density of the bulk sediment expressed as grams dry sediment/cm^3.

By setting the weight fraction, C_C, equal to unity, one calculates the bulk accumulation rate of the in situ dry bulk sediment. Accumulation rates were corrected for salt content by assuming a pore water salinity of 35‰ and calculating the weight fraction of salt (SA) from the equation

$$SA = \frac{X_W * (\text{salinity in } ‰/10^3)}{1 - X_W}$$

APPENDIX C

CANADIAN URANIUM REFERENCE ORE INTERCALIBRATION TO GE(Li) GAMMA DETECTOR

Canadian Uranium Reference Ore, BL-2. Canada Center for Minerals and Energy Technology, Dept. of Energy, Mines, and Resources.

Certified Values: pCi/g

Ra-226 (alpha spectrometry)	=1582	@ 102.4% efficiency
	=1545	@ 100 % efficiency (calc.)
Ra-226 (gamma spectrometry)	=1490±30	@ 96.2% efficiency
	=1549±31	@ 100 % efficiency (calc.)
Pb-210 (gamma spectrometry)	=1230	@ 82.6% efficiency
	=1489	@ 100 % efficiency (calc.)

Nuclide	Amount Determined, pCi/g ± S.D. (100 min counted interval)
	Canberra Geometry. Marinelli Beaker
Pb-214	1519 ± 49

APPENDIX D

CALCULATED U-238 CONCENTRATION IN CORE 20B (OC73-3-20)

Depth	U-235 Activity/gms dry sediment 143.6 KeV (dpm/gm dry sediment)	U-235 conc. μgm/ gm dry sediment (ppm)	Equivalent U-238 conc. μgm/ gm dry sediment (ppm)
MG3(0-15)	1.28 ± 0.44	0.270	37.2
MG3(15-30)	1.59 ± 0.45	0.336	46.2
MG3(30-45)	1.04 ± 0.38	0.220	30.3
MG3(45-60)	1.29 ± 0.35	0.272	37.4
MG3(60-75)	1.45 ± 0.37	0.301	41.4
P(60-75)	0.57 ± 0.39	0.120	16.5
P(160-175)	0.45 ± 0.39	0.095	13.1
P(200-215)	0.92 ± 0.42	0.194	26.7

Equivalent grams of U-238 calculated according to the equations:

$$\text{grams U-238} = 137.5 * \text{grams U-235}$$

and

$$\text{grams U-235} = \text{dpm U-235} * 2.11 \times 10^{-7}$$

APPENDIX E

BULK DENSITY DATA DETERMINED IN THIS STUDY

Core	Interval (cm)	Wet Bulk Density (grams wet sediment/cm^3)	Water Content (grams water/ grams wet sediment
Y73-4-34	MG(0-15)	1.5754 1.6592	0.4437 0.4410
	MG(15-25)	1.6903 1.6929	0.3964 0.3897
	MG(25-40)	1.6894 1.6622	0.3905 0.3940
	MG(43-58)	1.6633 1.6513	0.4123 0.4153
Y73-4-34	AAS Combined Sample (7.5, 20, 32.5, and 50.5)	AVG. 1.6605	AVG. 0.4104
Y73-4-40	MG(0-15)	1.4851 1.4881	0.5063 0.5034
	MG(17-32)	1.5038 1.5003	0.4933 0.5053
	MG(34-49)	1.5927 1.6027	0.4455 0.4491
	MG(51-66)	1.6320 1.5642	0.4612 0.4676
	MG(69-84)	1.5067 1.4957	0.4983 0.5047
Y73-4-40	AAS Combined Sample (7.5, 24.5, 41.5, 58.5 and 76.5)	AVG. 1.5371	AVG. 0.4835
OC73-3-30	MG(0-15)	1.4226 1.4411	0.5272 0.5446
	MG(15-27)	1.4618 1.4606	0.5204 0.5244
	MG(27-39)	1.4880 1.4781	0.5034 0.5187
	MG(39-54)	1.4590 1.4778	0.5095 0.5101

Core	Interval (cm)	Wet Bulk Density (grams wet sediment/cm^3)	Water Content (grams water/ grams wet sediment
OC73-3-30	AAS Combined Sample (7.5, 21, 33, and 46.5)	AVG. 1.4611	AVG. 0.5198
Y73-4-55	MG(0-12)	1.5082 1.5176	0.5021 0.5001
	MG(18-30)	1.5019 1.4727	0.5222 0.5238
Y73-4-55	AAS Combined Sample (6 and 24)	AVG. 1.5001	AVG. 0.5121
Y73-4-56	MG(0-12)	1.4753 1.4904	0.5213 0.5241
	MG(15-27)	1.3537 1.3684	0.5973 0.5983
	MG(31-43)	1.3543 1.3594	0.6305 0.6257
Y73-4-56	AAS Combined Sample (6, 21, and 37)	AVG. 1.4003	AVG. 0.5829
Y73-4-64K	(12-18)	1.359 1.348 1.352	0.6253 0.6120 0.6499
	(42-48)	1.3085 1.2829 1.2821	0.6680 0.6882 0.6917
	(72-78)	1.268 1.271 1.282	0.7050 0.6964 0.7009
Y73-4-64K	AAS Combined Sample (15, 45, and 75)	1.3059	0.6708

Core	Interval (cm)	Wet Bulk Density (grams wet sediment/cm^3)	Water Content (grams water/ grams wet sediment
OC73-3-25	MG(0-15)	1.4424 1.4297	0.5632 0.5669
	MG(15-29)	1.4920 1.4855	0.5159 0.5335
	MG(29-44)	1.4833 1.4972	0.5159 0.5201
	MG(44-59)	1.5107 1.4960	0.5225 0.5297
OC73-3-25	AAS Combined Sample MG(7.5, 22, 36.5, and 51.5)	AVG. 1.4796	AVG. 0.5335
OC73-3-20	MG(0-15)	1.2602 1.2373	0.6704 0.6544
	MG(15-30)	1.2418 1.2466	0.7311 0.7325
	MG(30-45)	1.3054 1.2802	0.6667 0.6720
	MG(45-60)	1.2801 1.2817	0.6583 0.6580
	MG(60-75)	1.2759 1.2818	0.6764 0.7062
	P(60-75)	1.2915 1.2992	0.6705 0.6591
	P(160-175)	1.2966 1.3239	0.6539 0.6458
	P(200-215)	1.2909 1.3018	0.6746 0.6690
OC73-3-20	AAS Combined Sample MG(7.5, 22.5, 37.5, 52.5, and 67.5) P(67.5 and 167.5)	AVG. 1.2809	AVG. 0.6749
OC73-3-16	MG(0-15)	1.5504 1.5720	0.4691 0.4592

Core	Interval (cm)	Wet Bulk Density (grams wet sediment/cm^3)	Water Content (grams water/ grams wet sediment
OC73-3-16 Cont'd.	MG(15-27)	1.5688 1.5524	0.4444 0.4295
	P(15-27)	1.5760 1.6628	0.4540 0.4479
	P(65-80)	1.5831 1.5752	0.4524 0.4519
	P(150-165)	1.5698 1.6045	0.4623 0.4606
OC73-3-16	AAS Combined Sample MG(7.5 and 21) P(21, 72.5, and 157.5)	AVG. 1.5815	AVG. 0.4531
OC73-3-8	MG(0-12)	1.3529 1.3620	0.6115 0.5930
	MG(12-24)	1.4815 1.5582	0.5279 0.4715
	MG(24-37)	1.5653 1.5361	0.4501 0.4610
	MG(37-50)	1.6050 1.4804	0.4289 0.5080
	MG(50-62)	1.6194 1.5903	0.4135 0.4323
OC73-3-8	AAS Combined Sample MG(6, 18, 30.5, 43.5, and 56)	AVG. 1.5151	AVG. 0.4898
OC73-3-6	MG(0-15)	1.3042 1.2932	0.6478 0.6656
	MG(17-29)	1.2696 1.2915	0.6823 0.6403
	MG(31-43)	1.2576 1.2954	0.6937 0.6678
	MG(45-57)	1.2529 1.2858	0.6843 0.6747

Core	Interval (cm)	Wet Bulk Density (grams wet sediment/cm^3)	Water Content (grams water/ grams wet sediment
OC73-3-6 Cont'd.	MG(59-71)	1.3089	0.6567
		1.2839	0.6439
	MG(94-106)	1.2511	0.6768
		1.2699	0.6646
OC73-3-6	AAS Combined Sample MG(7.5, 23, 37, 51, 65, and 100)	AVG. 1.2803	AVG. 0.6665
Y73-3-21K	MG(8-14)	1.1867	0.7601
		1.1767	0.7597
		1.1869	0.7641
	MG(32-38)	1.2009	0.7565
		1.1815	0.7524
		1.1905	0.7518
	MG(58-64)	1.1680	0.7662
		1.1931	0.7770
		1.1915	0.7660
Y73-3-21K	AAS Combined Sample MG(11, 35, and 61)	AVG. 1.1863	AVG. 0.7615

APPENDIX F

COCCOLITH NANNOFOSSIL STRATIGRAPHY RESULTS

Core Interval with Coccolith Stratigraphic Time Zone		Interval over which Sedimentation Rate was Determined	
OC73-3-6P			
300 cm (Middle and late Miocene, mixed)	?14.0-15.0 my		
635 cm (Middle Miocene)	14.0-15.0 my	0-635 cm	0.04-0.05 cm/10^3yrs
OC73-3-16P			
158 cm (Quaternary)	0.2-0.9 my	0-158 cm	0.18-0.79 cm/10^3yrs
213 cm (Quaternary)	0.9-1.6 my	0-213 cm	0.13-0.24 cm/10^3yrs
OC73-3-25P			
52 cm (Quaternary)	0.2-0.9 my		
157 cm (Quaternary)	0.2-0.9 my	0-157 cm	0.17-0.79 cm/10^3yrs
OC73-3-30P			
35 cm (Quaternary)	0.2-0.9 my	0-35 cm	0.04-0.18 cm/10^3yrs
158 cm (Quaternary)	1.6-1.8 my	0-158 cm	0.09-0.10 cm/10^3yrs
Y73-4-40			
40P 75 cm (Quaternary)	0.2-0.9 my	0-75 cm	0.08-0.38 cm/10^3yrs
OC73-3-20			
MG5 1 cm - surface (Quaternary)	0.2-0.9 my		
20P 230 cm (Quaternary)	0.2-0.9 my	0-230 cm	0.26-1.15 cm/10^3yrs

APPENDIX G

SEDIMENTATION RATE COMPILATION

FOR THE

SOUTHEAST PACIFIC OCEAN

CORE	LAT. LONG.	DEPTH (m)	SED. RATE (cm/10^3yrs)	METHOD	REFERENCE
OC73-3-6	20°03.3'S 95°17.7'W	4309	0.26	$^{230}Th_{xs}$	this study
OC73-3-8	18°08'S 102°01'W	4090	0.16	$^{230}Th_{xs}$	this study
OC73-3-16	20°18.8'S 113°14.4'W	3156	0.40	$^{230}Th_{xs}$	this study
			0.44	Thickness/ Age	this study
OC73-3-25	20°00.0'S 114°31.0'W	3247	0.39	$^{230}Th_{xs}$	this study
OC73-3-20	19°14.9'S 113°34.5'W	3081	1.91	$^{230}Th_{xs}$	this study
			3.35	Thickness/ Age	this study
Y73-3-21K	13°36.8'S 102°31.5'W	4410	0.13 (0.19)	$^{230}Th_{xs}$	this study
Y73-4-64K	32°46.4'S 94°42.0'W	3871	0.22 (0.43)	$^{230}Th_{xs}$	this study
Y73-4-56	32°38.8'S 102°16.1'W	3717	0.15	$^{230}Th_{xs}$	this study
Y73-4-55	32°38.1'S 105°54.8'W	3524	0.15	$^{230}Th_{xs}$	this study
N-2	32°21'S 105°55'W	(1980 fathoms)	0.18	$^{230}Th_{xs}$	this study recalculated from Urry (1949)
OC73-3-30	30°30.1'S 110°28.1'W	3003	0.28	$^{230}Th_{xs}$	this study
			0.35	Thickness/ Age	this study
Y73-4-40	31°07.2'S 112°26.3'W	2797	0.29	$^{230}Th_{xs}$	this study
Y73-4-34	31°09'S 113°21'W	3064	0.39	$^{230}Th_{xs}$	this study

CORE	LAT. LONG.	DEPTH (m)	SED. RATE (cm/10^3yrs)	METHOD	REFERENCE
DW-07	48°28.0'S 113°17.0'W	2580	1.67	^{18}O depth to 18K	CLIMAP (1977)
DWBG-30	19°50'S 148°39'W	4620	0.04	$^{230}Th/^{232}Th$	Goldberg & Koide (1962)
			0.09	Recalculated $^{230}Th/^{232}Th$	Ku et al. (1968)
DWBG-52	40°36'S 132°49'W	5120	0.05	$^{230}Th/^{232}Th$	Goldberg & Koide (1962)
			0.14	Recalculated $^{230}Th/^{232}Th$	Ku et al. (1968)
DWBG 98C	20°49'S 81°08'W	2300	0.69	$^{230}Th/^{232}Th$	Blackman & Somayajulu (1966)
DWBG 114	18°20'S 79°21'W	3090	0.61	$^{230}Th/^{232}Th$	Blackman & Somayajulu (1966)
DWHG 49	42°02'S 98°01'W	4359	0.04	$^{230}Th/^{232}Th$	Goldberg & Koide (1962)
			0.06	Recalculated $^{230}Th/^{232}Th$	Ku et al. (1968)
E11-02	56°04.4'S 115°05.6'W	3109	7.78	^{18}O depth to 18K	CLIMAP (1977)
E11-03	56°54.2'S 115°14.6'W	4023	3.33	^{18}O depth to 18K	CLIMAP (1977)
E11-04	57°49.7'S 115°12.5'W	4773	0.89	^{18}O depth to 18K	CLIMAP (1977)
E15-06	59°58.0'S 101°19.0'W	4517	1.50	^{18}O depth to 18K	CLIMAP (1977)
E15-12	58°41.0'S 108°48.0'W	4572	1.67	^{18}O depth to 18K	CLIMAP (1977)
E20-18	44°23'S 111°20'W	2868	1	$^{230}Th_{xs}$ (equil. level)	Geitzenauer (1972)
E21-14	49°02'S 120°05'W	3319	.9	$^{230}Th_{xs}$ (equil. level)	Geitzenauer (1972)

CORE	LAT. LONG.	DEPTH (m)	SED. RATE (cm/10^3yrs)	METHOD	REFERENCE
KK71-GC 07	10°33'S 83°02'W	4514	0.23	$^{230}Th_{xs}$	McMurtry & Burnett (1975)
KK71-106GC 10	09°59'S 106°02'W	3447	0.43	$^{230}Th_{xs}$	Dymond & Veeh (1975)
KK71-FFC 109	12°05'S 110°37'W	3069	1.08	$^{230}Th_{xs}$	McMurtry & Burnett (1975)
KK71-FFC 115	11°58'S 103°23'W	4548	0.19	$^{230}Th_{xs}$	McMurtry & Burnett (1975)
KK71-FFC 132	11°33'S 97°27'W	3996	0.07	$^{230}Th_{xs}$	McMurtry & Burnett (1975)
OC73-3-27	21°00.7'S 114°43.9'W	3309	0.61 (avg)	Thickness/ Age	this study
RC8-92	31°33'S 108°30'W	2710	0.30	Correlation of frequency curve for G. menardii with RC8-93 RC8-94	Ericson & Wollin (1970)
RC8-93	29°22'S 105°14'W	3157	0.35	Paleomag. and $^{230}Th_{xs}$	Ku et al. (1968)
			0.36	Paleomag.	Glass et al. (1967) Cited by Ericson & Wollin (1970)
RC8-94	27°17'S 102°05'W	3075	0.18	Paleomag.	Ericson & Wollin (1970)
RC9-99	24°36'S 115°27'W	2570	0.70	Paleomag.	Glass et al. (1967)
RC11-227	5°59'S 114°37'W	——	0.81	Paleomag. B/M	
RC11-230	08°48'S 110°48'W	3259	2.53	^{18}O depth to 18K	CLIMAP (1977)
			1.92 - 2.30	^{14}C($\frac{28\text{-}32 \text{ cm}}{14.28 \pm 0.32 \times 10^3 \text{yrs}}$)	CLIMAP (1977)

CORE	LAT. LONG.	DEPTH (m)	SED. RATE (cm/10^3yrs)	METHOD	REFERENCE
RC13-113	01°39'S 103°38'W	3195	2.81	Fauna Correlation to ^{18}O depth to 18K	Molina-Cruz (1978)
RC13-140	2°51'S 87°45'W	2202	3.6	Ash layer plus S. Universus extinction	Ninkovich & Shackleton (1975)
RC15-61P	40°36'S 77°12'W	3771	3.78	^{18}O depth to 18K	Molina-Cruz (1978)
V15-32	3°15'S 82°30'W	2796	2.6	Ash layer plus S. Universus extinct.	Ninkovich & Shackleton (1975)
V15-33	6°08'S 82°41'W	3947	4.5	Ash layer plus S. Universus extinct.	Ninkovich & Shackleton (1975)
V15-39	10°05'S 80°58'W	4654	1.1	Ash layer plus S. Universus extinct.	Ninkovich & Shackleton (1975)
V15-42	7°36'S 81°47'W	4459	2.6	Ash layer plus S. Universus extinct.	Ninkovich & Shackleton (1975)
V15-53P	33°27'S 73°40'W	3915	2.22	^{18}O depth to 18K	Molina-Cruz (1978)
V17-44	3°34'S 85°07'W	3285	2.9	Ash layer plus S. Universus extinct.	Ninkovich & Shackleton (1975)
V19-27	00°28'S 82°40'W	1350	3.6	Ash layer plus S. Universus extinct.	Ninkovich & Shackleton (1975)
V19-28	2°22'S 84°39'W	2666	3.8	Ash layer plus S. Universus extinct.	Ninkovich & Shackleton (1975)

CORE	LAT. LONG.	DEPTH (m)	SED. RATE (cm/10^3yrs)	METHOD	REFERENCE
V19-29	3°35'S 83°56'W	3091?	5.7	Ash layer plus S. Universus extinct.	Ninkovich & Shackleton (1975)
		3157?	6.69	^{18}O depth to 18K	Molina-Cruz (1978)
V19-30	3°23'S 83°31'W	3027	5.5	Ash layer plus S. Universus extinction	Ninkovich & Shackleton (1975)
V19-41	14°05'S 96°12'W	3248	1.69	^{18}O depth to 18K	CLIMAP (1977)
V19-53	17°01'S 113°31'W	3058	2.11	^{18}O depth to 18K	CLIMAP (1977)
V19-54	17°02'S 114°54'W	2830	1.50	$^{230}Th_{xs}$	Bender et al. (1971)
V19-55	17°00'S 114°11'W	3177	1.11	^{18}O depth to 18K	CLIMAP (1977)
V19-61	16°57'S 116°18'W	3407	0.70	$^{230}Th_{xs}$	Bender et al. (1971)
V19-64	16°56'S 121°12'W	3540	0.45	$^{230}Th_{xs}$	Bender et al. (1971)
			0.72	^{18}O depth to 18K	CLIMAP (1977)
V21-30	01°13.0'S 86°40.0'W	617	13.89	^{18}O depth to 18K	CLIMAP (1977)
			12.98-13.81	$^{14}C(\frac{199\text{-}202\text{cm}}{14.98 \pm 0.35\times10^3\text{yrs}})$	CLIMAP (1977)
V21-33P	03°48'S 92°05'W	3726	2.58	^{18}O depth to 18K	Molina-Cruz (1978)
V21-48	09°31'S 126°22'W	3922	0.50	Paleomag. B/M	Glass et al. (1967)
			0.50	$^{230}Th_{xs}$	Ku et al. (1968)

CORE	LAT. LONG.	DEPTH (m)	SED. RATE (cm/10^3yrs)	METHOD	REFERENCE
Y69-71P	00°06'N 86°29'W	2740	9.75	^{18}O depth to 18K and ^{14}C	Molina-Cruz
Y71-6-12P	16°26'S 77°34'W	2734	1.36	^{18}O depth to 18K	Molina-Cruz
Y71-7-36MG2	10°08'S 102°51'W	4541	0.14	$^{230}Th_{xs}$	Dymond & Veeh (1975)
Y71-7-44	10°42'S 110°01'W	3167	1.28	Thickness/ Age	this study
Y71-7-45P	11°05'S 110°06'W	3096	0.93	$^{230}Th_{xs}$	Dymond & Veeh (1975)
			0.50	^{18}O depth to 18K	
			0.85	Thickness/ Age	this study
Y71-7-47	11°18'S 110°06'W	3188	0.76	Thickness/ Age	this study
Y71-7-48	11°20'S 110°11'W	3128	1.18	Thickness/ Age	this study
Y71-7-52	10°43'S 110°42'W	3198	0.73	Thickness/ Age	this study
Y71-7-53	10°52'S 110°44'W	3180	1.36	Thickness/ Age	this study
Y73-3-13MG3 DSDP Site 319	12°59.0'S 101°33.05'W	4303	0.11	micro-paleontology	Dymond et al. (1977)